Global and Planetary Change 176 (2019) 1–22

Contents lists available at ScienceDirect

Global and Planetary Change

journal homepage: www.elsevier.com/locate/gloplacha

Research article

The influence of centennial-scale variations in the South American summer monsoon and base-level fall on Holocene fluvial systems in the Peruvian Andes

Willem Viveen[a,*], Leonardo Zevallos-Valdivia[a,b], Jorge Sanjurjo-Sanchez[a,c]

[a] Grupo de Investigación en Geología Sedimentaria. Especialidad de Ingeniería Geológica, Departamento de Ingeniería, Pontificia Universidad Católica del Perú, San Miguel, Lima, Peru
[b] Universidad Nacional de San Agustin de Arequipa, Facultad de Geología, Geofisica y Minas, Arequipa, Peru
[c] Instituto Universitario de Geología "Isidro Parga Pondal", Universidad de A Coruña, A Coruña, Spain

ARTICLE INFO

Keywords:
Fluvial terrace
Climate change
Andes
Sediments
Geomorphology
Stratigraphy

ABSTRACT

The occurrence of Holocene changes in the South American Summer Monsoon (SASM) in the Peruvian Andes has been well established in paleoclimatological records such as speleothem, lake and glacier records. How river systems responded to these events has, however, hardly been investigated. Here, we present evidence based on sedimentological, stratigraphical and geomorphological data as well as radiometric (optically stimulated luminescence and radiocarbon) dating that rivers from the Peruvian Andes are extremely sensitive to changes in SASM activity. The presence of lake sediments shows that from at least 12,000 years ago until 4153 ± 988 years ago a lake was present in the Mantaro River valley, possibly due to damming by a glacier or glacial landforms. A reconstruction of fluvial terrace profiles shows that 4418 ± 500 years ago the Mantaro and its tributary, the Cunas River, incised and laid down sediments simultaneously as a response to changes in regional base-level and increased SASM activity. The latter was largely subdued during a large part of the Holocene as evidenced by paleoclimatological records in the region. Between 2245 ± 217 years ago and the present, the frequency of SASM events increased drastically and both rivers formed the majority of their fluvial terraces. In total, over the past ~4000 years, the Mantaro River formed five terrace levels and the Cunas River formed seven main terraces. Locally, 11 terrace levels were recognised. Terrace formation occurred at intervals of approximately 250 to 300 years between 2245 ± 217 and 1188 ± 60 years ago and approximately every 150 years after 824 ± 66 years ago until the present. A comparison with paleoclimatological data shows that sedimentation events correlate to periods of increased precipitation and glacier retreat in the Peruvian Andes, whereas phases of incision are attributed to continuous adjustments in base-level fall. Thirty-four metres of incision has occurred since 4418 ± 500 years ago averaging 7.7 mm yr^{-1}. A comparison with data from other river systems in the Peruvian Andes shows that many rivers responded in a similar way to centennial-scale variations in SASM activity. Fluvial activity is thus not related to interannual variations in the El Niño Southern Oscillation (ENSO) contrary to previous proposals.

1. Introduction

Fluvial terraces are a valuable source of information on how landscapes responded to climatic and tectonic changes (Bridgland and Westaway, 2008a). This is especially true for Peru, one of the countries with the largest amount of fresh water in the world. Peru also experiences one of the largest contrasts in regional climates, ranging from hyper-arid to wet tropical, as well as large contrasts in topographic elevation between the Amazon lowlands and the Andes. Yet, how Peru's river systems responded to long-term changes in climate and topography remains poorly understood. Fluvial terrace research has traditionally focused on the southern Peruvian coast and foothills where rapid tectonic uplift has preserved well-developed terrace staircases of two to three terraces levels (Bekaddour et al., 2014; Steffen et al., 2009). In most cases, the terrace sediments are of late Pleistocene age and were deposited under a regime of increased river discharge controlled by precessional forcing (Litty et al., 2018). The timing of deposition of fluvial sediments during the late Pleistocene and early

* Corresponding author.
E-mail address: wviveen@pucp.pe (W. Viveen).

https://doi.org/10.1016/j.gloplacha.2019.03.001
Received 21 December 2018; Received in revised form 28 February 2019; Accepted 1 March 2019
Available online 04 March 2019
0921-8181/

Holocene generally corresponded to lake-level highstands on the Altiplano, suggesting an increase in precipitation (Baker et al., 2001a; Rigsby et al., 2003). Deposition and characterisation of fluvial sediments is also the result of intrinsic changes in the river basins themselves (Veldkamp et al., 2017; Vandenberghe et al., 2018), for instance by headward erosion resulting in changes in sediment provenance areas (Litty et al., 2017a), emptying of differential sediment reservoirs (Steffen et al., 2010) or by changes in threshold conditions of basin slope and water flux (Litty et al., 2017b). Downcutting of the fluvial systems and the actual formation of terrace surfaces and scarps has been linked to increased discharge in combination with reduced fluvial sediment load (Steffen et al., 2009; Litty et al., 2018) or a lowering in base-level, either by lake emptying (Rigsby et al., 2003) or tectonic uplift (Viveen and Schlunegger, 2018). Outside of the southern Peruvian coastal areas and the Altiplano, however, very little is known about the response of fluvial systems to external changes. One reason could be that the coast north of Lima is tectonically subsiding, thereby impeding fluvial incision through base-level fall and the formation of fluvial terraces (Viveen and Schlunegger, 2018). Even less is known about the Holocene period, and what is known about fluvial sedimentation is generally explained by mechanisms involving El Niño Southern Oscillation (ENSO), e.g. Wells (1990), Keefer et al. (2003), Magilligan et al. (2008), Sandweiss et al. (2009), Abbühl et al. (2010). ENSO is characterised by interannual variations in air temperature and discharge, yet in the instrumental record there is no clear correlation between flooding, precipitation and ENSO events (Garreaud et al., 2009; Baker and Fritz, 2015). Over timescales spanning millennia, as registered in Peruvian Andean speleothems, there is no clear relationship between increased precipitation and ENSO-forcing either (Kanner et al., 2013). It is also striking that the few existing fluvial records of the late Holocene with reasonable age control show cyclicity in depositional patterns of centuries to millennia (Wells, 1990; Rigsby et al., 2003; Rein et al., 2004, 2005; Magilligan et al., 2008). This is at odds with the interannual cyclicity that characterises ENSO (Garreaud et al., 2009) and, as such, questions the validity of an ENSO control on fluvial sedimentation over timescales spanning centuries to millennia.

For those reasons we aim to find an answer as to what climatic signal controls fluvial terrace formation during the Holocene. A second objective is to present fluvial terrace data from the central Peruvian Andes because this vast region has not yet received attention from the scientific community. The present study focuses on the Huancayo tectonic basin (11° S latitude), situated in the Peruvian central Andes (Fig. 1). Here, the Mantaro and Cunas Rivers have formed flights of well-preserved fluvial terraces. The Mantaro terraces are considered to have formed under orbitally-driven changes in Pleistocene climate (Mégard, 1968) and the basin experiences active deformation as evidenced by seismic activity (Dorbath et al., 1990; Tavera, 2017). We will present results of geomorphological mapping, sedimentological and stratigraphical analysis as well as ^{14}C and Optically Stimulated Luminescence Dating (OSL) of fluvial terrace sediments. As the Cunas and Mantaro terraces are cut into underlying basin fill, an important part of this paper will be dedicated to identifying what is fluvial terrace sediment and what is not. Then, correlations between the terraces of both rivers will be established in order to capture a regional signal controlling both river systems. Subsequently a chronological framework will be established after which a discussion follows about climatic and other factors controlling fluvial terrace development. The paper ends with a comparison of our data with those of other Andean river systems.

2. Study area

The Huancayo basin is an intramontane basin that is situated in between the eastern cordillera and the high plateau of the Peruvian central Andes (Fig. 1; Marocco et al., 1995). The Huancayo basin was probably initiated during the late Miocene, as suggested by ^{40}Ar / ^{39}Ar-dating of volcanic ash in the basal part of the Huancayo basin fill (Wise, 2007). Recent folding has been observed along the western basin border (Mégard, 1968; Dorbath et al., 1990; Wise, 2007), whereas faults and folds have not been recognised along the eastern basin border (Dorbath et al., 1990). The infill of the Huancayo basin (Figs. 2 and 3) is characterised by yellowish, matrix-supported, pebble conglomerates and sandstones of the upper Miocene Ushno Fm (Blanc, 1984). The Mataula Fm is lying unconformably above the Ushno Fm (Fig. 3) and is made up of lacustrine siltstones as well as cross-stratified sandstones with interbedded pebbles. In the eastern part of the Huancayo basin two distinct alluvial fan sequences were recognised. The Torre Torre conglomerates are the oldest of these and have a possibly upper Pliocene to lower Pleistocene age (Wise, 2007). The second alluvial fan sequence underlies the city of Huancayo and is of an undifferentiated Pleistocene age (Wise, 2007). In the southwestern corner of the basin, a sequence, at least 60 m thick, of massive conglomerates interbedded with sand lenses is found. The section is most prevalent around the village of Chupaca and is thus named “the Chupaca gravels” (Wise, 2007). The deposits are folded, forming open anticlines, up to 60 m high. The gravels have been interpreted as fluvio-glacial deposits or glacis belonging to various Pleistocene glacial periods (Mégard, 1968). Alternatively, they have been interpreted as purely fluvial sediments of the Mantaro River (Blanc, 1984). Wise (2007) considered the facies to be fluvial but not related to the Mantaro River, as its base is located on top of the upper Miocene Mataula Fm and folding of the sediments suggests a far earlier, possibly Pliocene, age. We follow here the age proposed by Wise (2007). The Huancayo alluvial fan and the Chupaca gravels are located at a maximum of 50 m to 70 m above the Mantaro River and cut by three levels at 50 m (T1; see Fig. 2), 14–20 m (T2) and 4–8 m (T3) above the current floodplain (Harrison, 1943). As such, Wise (2007) suggested that the Mantaro terraces at 4–8 m and 14–20 m are younger than the Huancayo fan and Chupaca gravels and of Pleistocene age. The Cunas River terraces, on the other hand, have not yet been described by other workers.

The Mantaro River catchment encompasses 34,363 km^2. The Mantaro River originates in Lake Junín at 4080 m above sea level (a.s.l.), just north of the city of Junín (Fig. 1). The Mantaro River is 768 km long and connects to the Apurimac River further south at 4800 m a.s.l. (Ministerio de Agricultura and ANA, 2013). The catchment contains several glaciated peaks as high as 5496 m a.s.l (Figs. 1 and 2). In the Huancayo basin itself, the river runs at 3300 to 3200 m a.s.l. Discharge is dependent on rainfall and is highly seasonal, with peak discharges, as measured at a weir station in Jauja, of up to 310 $m^3 s^{-1}$ in the months March to May and discharges ranging from 30 $m^3 s^{-1}$ to 100 $m^3 s^{-1}$ in the other months (Ministerio de Agricultura and ANA, 2013). Annual rainfall is around 800 mm yr^{-1} (Ministerio de Agricultura and ANA, 2013).

The Cunas River has a catchment area of 1718 km^2 (Ministerio de Agricultura, ANA, 2010) with its headwaters located at 5180 m a.s.l. It flows for 99 km (Ministerio de Agricultura and ANA, 2013) before joining the Mantaro River at 3185 m a.s.l. The Cunas River has a mean annual discharge of 16 $m^3 s^{-1}$ that fluctuates between 3 $m^3 s^{-1}$ in the dry season and 28 $m^3 s^{-1}$ in the wet season.

The present study focuses on the southwestern part of the Huancayo basin (Fig. 1). Here, the Cunas River runs perpendicular to the basin axis and cuts through the Mantaro River terraces. The incision of the Cunas valley increases from approximately 8 m close to the confluence with the Mantaro River to over a hundred metres at the folded, western basin border.

3. Regional climate

During the meridional summer the Intertropical Convergence Zone (ITCZ) shifts to its most southward position and pushes the eastern trade winds southward. During this time the easterlies transport moisture from the Atlantic across the Amazon basin, which condenses and rains out in the Andes, forming the South American Summer

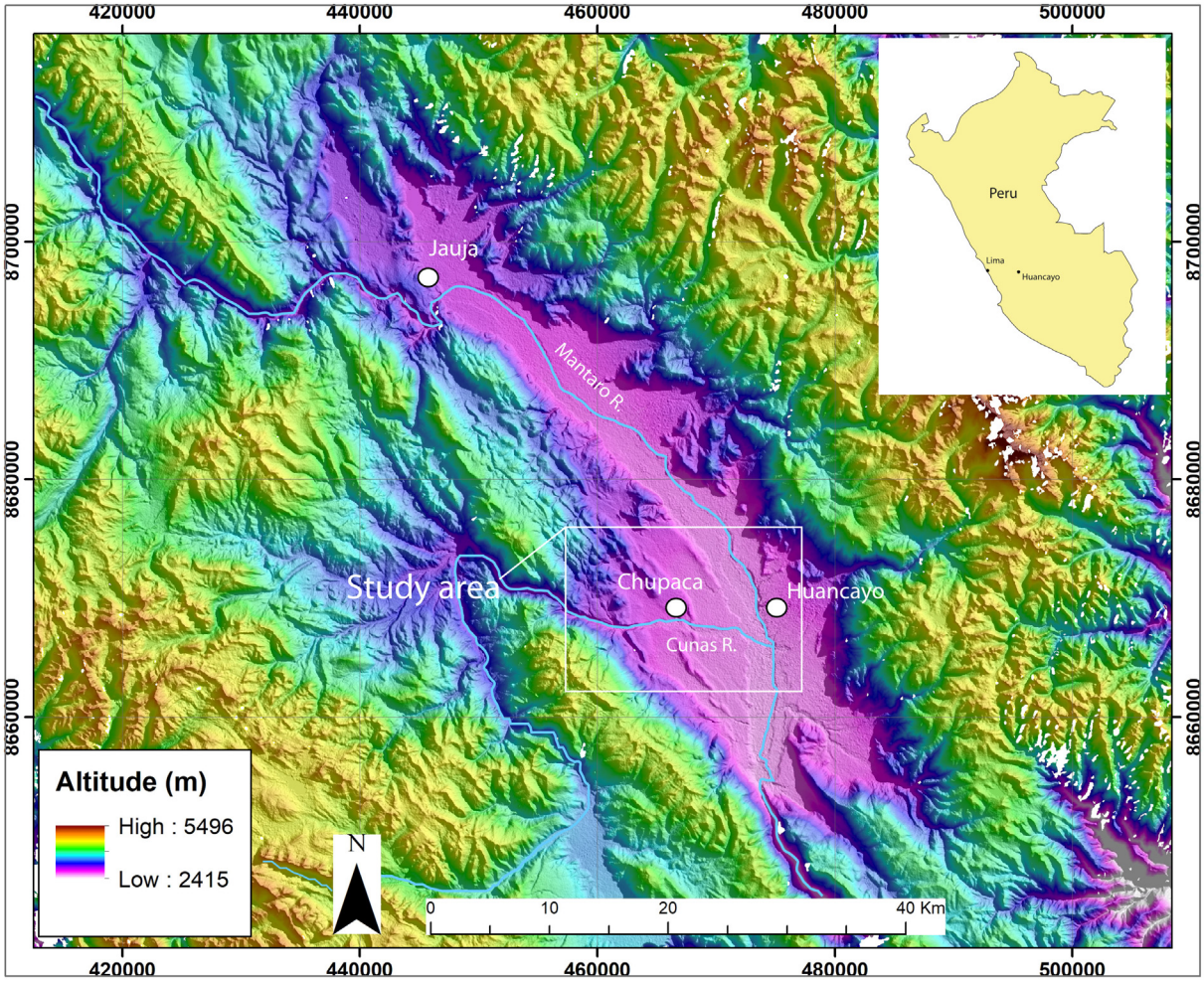

Fig. 1. Study area.

Monsoon (SASM; Garreaud et al., 2003). The SASM is partly influenced by the El Niño Southern Oscillation (ENSO), which is characterised by interannual variations in temperature and precipitation due changes in sea surface temperature (SST) of the Pacific Ocean (Garreaud et al., 2003). The SST typically rises when the Equatorial ocean currents shift south and heat up the colder waters of the Humboldt Current in northern Peru. In La Niña years an intensification of the wind circulation in the upper atmosphere increases the intensity of the easterlies and rain out in the Andes (Garreaud et al., 2003). During El Niño years the easterlies are weaker and give way to the drier westerlies, thereby decreasing rain out over the Andes. Over timescales spanning decades to centuries, Atlantic SST plays an important role. Drops in equatorial Atlantic SST and associated increases in the strength of the easterlies coincide with a more intense SASM (Nobre and Shukla, 1996). Teleconnections exist between the tropical and high-latitude Atlantic as drops in SST of the former are significantly correlated to increases in Arctic ice cover (Hurrell and van Loon, 1997; Seager et al., 2000; Chiang and Bitz, 2005). Stable isotopes in carbonate sediments in Andean lakes show large variations in precipitation in concordance with fluctuations in Atlantic SST over the past few millennia, caused by precessional forcing (Vuille et al., 2012; Baker and Fritz, 2015). Stable isotopes from other paleoclimatic archives show that Holocene climate was relatively warm and wet until 9000 years ago, then colder and drier until 4000 years ago (Seltzer et al., 2000; Bird et al., 2011; Stansell et al., 2013), and again warmer with more precipitation during the past 4000 years (Rein et al., 2005). The last two millennia are characterised by a higher frequency of ENSO events (Kanner et al., 2013).

4. Methodology

4.1. Terrace mapping sedimentological and stratigraphical descriptions

The fluvial terraces of the Cunas River were investigated from the confluence with the Mantaro River extending 13 kms upstream. They were first mapped using satellite images at a scale of 1:7500. The images were obtained by printing pairs of Google Earth images set at the maximal vertical exaggeration of 3 and analysed using a stereoscope. Based on the preliminary mapping, transects spaced 500 m apart, oriented perpendicular to the river and traversing the identified terraces were validated in the field. The position and altitude above the floodplain (+FP) of the terraces was registered with a Garmin handheld GPS with a barometer-based altimeter. Each transect was concluded in approximately 45 min. We assumed that during this short time the air pressure did not vary significantly and that the reading of the relative altitude between terraces within a transect was not biased by air pressure fluctuations. In tandem with terrace mapping using the satellite images and field reconnaissance a polygon terrace map was drawn in ArcGIS 10. Correlating the different terrace fragments was straightforward, as the majority of the terrace levels represented easily recognisable, continuous surfaces.

Using the ArcGIS-based terrace map, longitudinal profiles of the identified terrace levels were constructed. As a base line on which to project the terrace threads, we extracted the altitudes of the floodplain, at locations identified in the field, from the SRTM30 m Digital Elevation Model (DEM). A comparison between DEM-based elevation data and

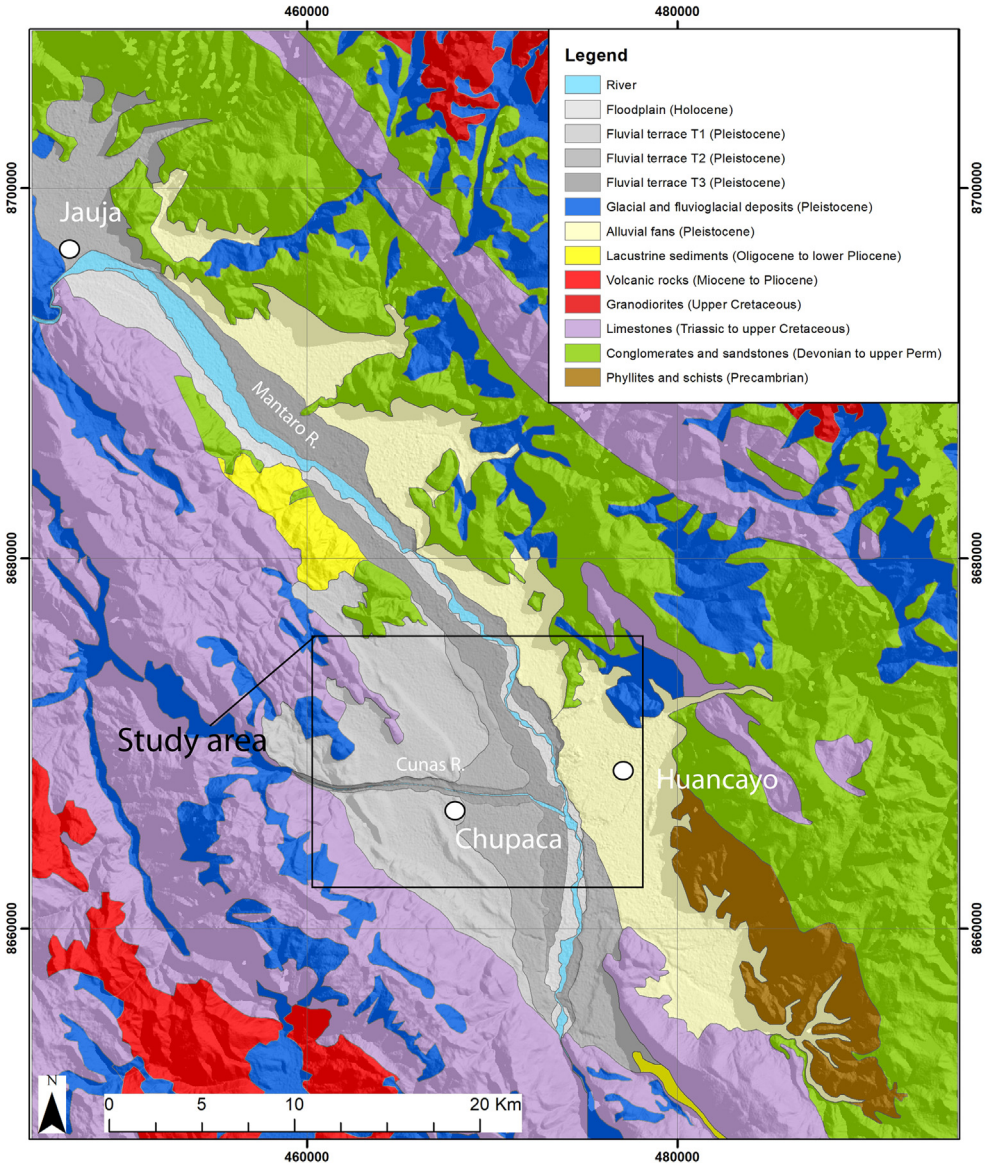

Fig. 2. Simplified geological map of the Huancayo basin based on Paredes (1970), Quispesivana and Navarro (2002) and Wise (2007).

high-resolution elevation data obtained by differential GPS measurements shows a mean absolute error of 3.3 m for the SRTM30 m of our study area (Gonzalez-Moradas and Viveen, unpublished data). This small error is acceptable for our purposes, as it will not alter the shape of the floodplain longitudinal profile.

The Mantaro River terraces were primarily mapped using the SRTM30 m DEM in combination with Microsoft Bing imagery. At selected locations in the field the presence of the mapped terraces was validated (Transect A-A´). We justify this approach because the Mantaro River terraces represent very large, continuous surfaces that were easily identified on satellite imagery.

Stratigraphical descriptions of the fluvial terraces were made using the lithofacies and facies association classification of Miall (1996). These served a twofold purpose:

i) To distinguish the sediments of the Cunas River from the older, underlying sediments. This was important because the OSL and ^{14}C ages needed to be placed in a proper stratigraphical context and we needed to make sure that we sampled fluvial terraces for dating purposes and not older, underlying sediments;
ii) To improve existing interpretations regarding depositional environments of the investigated facies.

4.2. Sampling

We concentrated the sampling in the Cunas River valley close to the confluence with the Mantaro River (Transect B-B´; Fig. 4), and at the upstream end of the Cunas River valley (Transect C-C´; Fig. 4). Some 25 samples for Optically Stimulated Luminescence (OSL) and ^{14}C dating were collected by hammering 30-cm long and 6-cm wide steel cylinders horizontally in fine-to-medium-grained sand lenses. All sand lenses were at least 30 cm thick. In the case of landforms that were geomorphologically recognisable as fluvial terraces, samples were collected in the top sections of the stratigraphical column (e.g. upper four metres) but not deeper, so as to prevent sampling of sediments that were deposited long before fluvial terrace formation (e.g. basin fill). Samples were taken from sand lenses located within gravel bodies or from sand bodies with a clear fluvial imprint, as evidenced for instance by cross-stratified sands. In the downstream section, we additionally sampled the valley wall from the bottom, where the Cunas River flows, all the way to the valley rim. The Cunas valley is cut into an older Mantaro terrace (Fluvial terrace T2 in Fig. 2) and the valley wall therefore

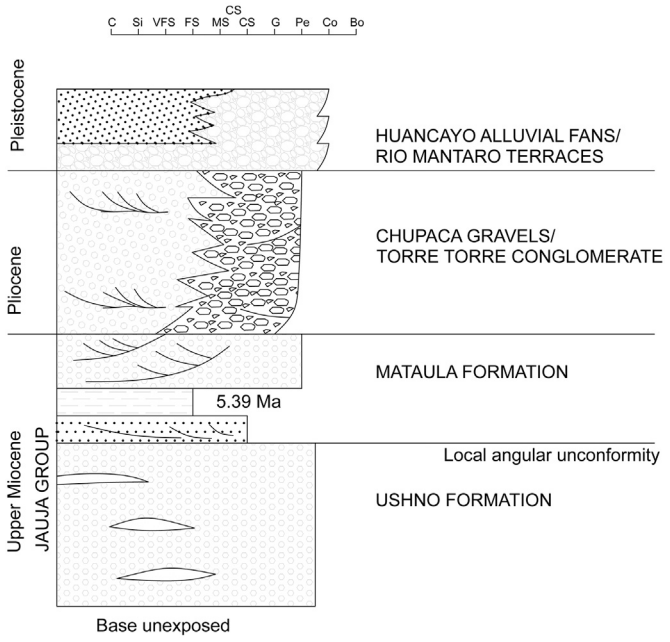

Fig. 3. Stratigraphical column of the Huancayo basin (based on Wise, 2007).

represents a complete stratigraphical column of this Mantaro terrace level. In this way we hoped to gain a better understanding of the evolution of the Mantaro valley before the Cunas River valley was formed. We also took two samples from two different, younger Mantaro River terraces. To avoid a potential influence from the Cunas River, the samples were taken between 5 and 10 km north of the Mantaro-Cunas confluence (Fig. 4).

4.3. Optically stimulated luminescence dating

The obtained cores were opened in the luminescence laboratory of the University of A Coruña under subdued red light. Quartz grains from the central part of the cores were obtained by procedures described in Viveen et al. (2014a). The quartz OSL signal was measured in an automated Risø DA-15 TL/OSL reader system equipped with blue (470 ± 30 nm) light-emitting diodes (LEDs) for stimulation. OSL signals were recorded with a coupled 9235QA photomultiplier tube (PMT). An optical 6 mm-thick Hoya U-340 filter was placed between the aliquots and the PMT. Laboratory doses were given using a $^{90}Sr/^{90}Y$ beta source mounted on the reader emitting a 0.120 ± 0.003 Gy s^{-1} dose. For measurements, although dim OSL signals were observed, small multi-grain aliquots were prepared. For some samples, the obtained signals and equivalent doses (D_e) of multi-grain aliquots of ~10–20 grains and ~100 grains were compared. The blue-OSL (BL-OSL) single-aliquot regenerative dose (SAR) protocol (Murray and Wintle, 2000) was used to estimate the D_es. Variable preheat temperatures among samples (from 200 to 240 °C) were chosen after performing preheat temperature tests. Dose recovery tests (Murray and Wintle, 2003) were also performed for all samples on bleached aliquots.

The natural dose-rate (D_r) was estimated in the laboratory using Low Background Gamma Spectrometry on bulk samples, measuring the ^{238}U, ^{235}U, ^{232}Th and ^{40}K decay chain activities. Gamma spectrometry was performed in the University of Seville (Spain) using Marillelli beakers with a coaxial Camberra XTRA gamma detector (Ge Intrinsic) within a 10 cm-thick lead shield. The relative efficiency was at 60% and at a resolution of 1.4 keV and 2.3 keV for energies 122 keV and 1332 keV, respectively.

To calculate the dose-rates, the conversion factors of Guerin et al. (2011) were used. The beta dose-rate was corrected (Brennan, 2003) due to an HF etching step. This step was necessary to obtain pure quartz grains by removal of the surface layer of the grains. The average water content of the samples was assessed considering both their maximum and measured water content as well as the depth of the samples in the

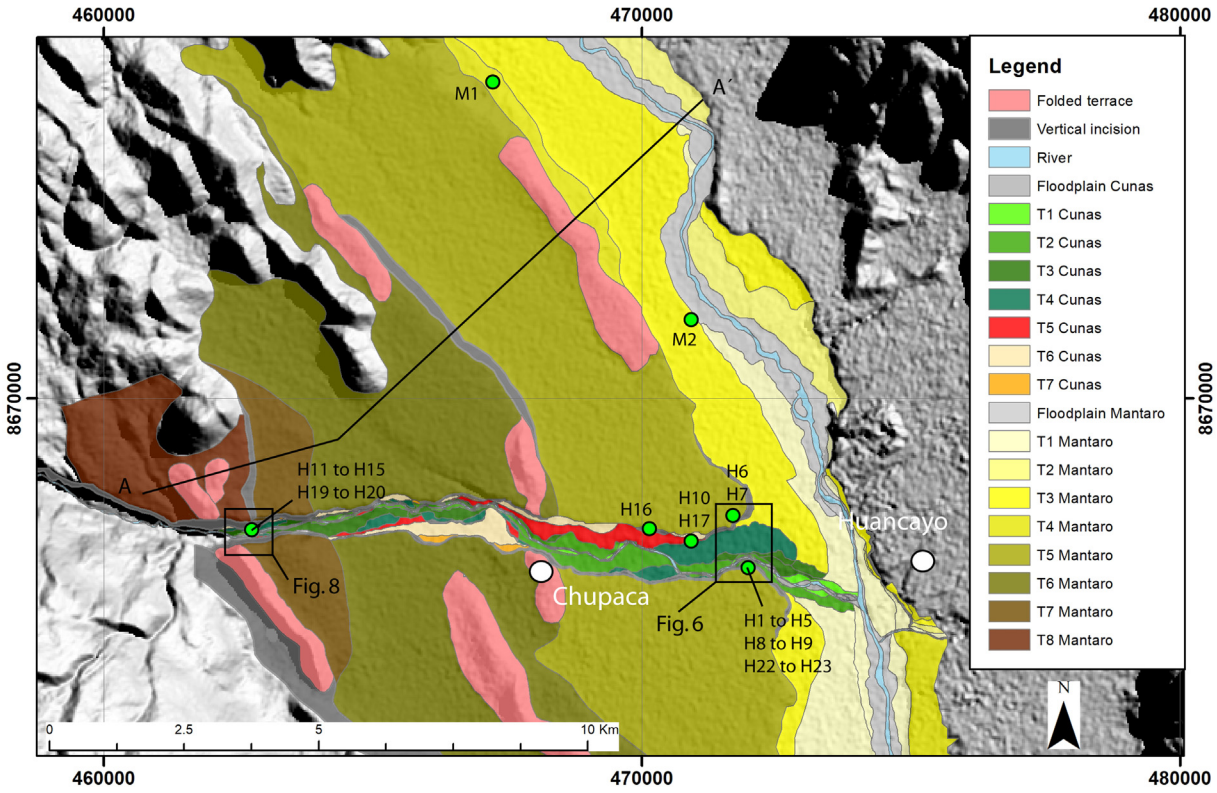

Fig. 4. Fluvial terrace map of the Mantaro and Cunas Rivers. Including Cunas (H1 to H23) and Mantaro (M1 and M2) OSL and ^{14}C sample locations.

sedimentary profiles in the field. The cosmic dose rates were calculated according to Prescott and Hutton (1994), but considering the geomorphologic evolution of the studied area an average cosmic dose was assumed for some of the samples.

4.4. Radiocarbon dating

Of the 25 samples collected in the field for OSL analysis, eight sand samples containing organic matter were selected for radiocarbon dating. The nature of the organic matter could not be verified by visual means. We therefore measured the C:N ratio and $\delta^{13}C$ of the organic matter to assess its origin (Deines, 1980; Wang et al., 1998; Accoe et al., 2002; Howard et al., 2009). For the age assessment, the samples were measured by means of an accelerator mass spectrometer of the laboratory of the International Chemical Analysis (ICA) in Florida (USA). The ages were calibrated using the Oxcal 4.1 software package (Bronk Ramsey and Lee, 2013) based on the calibration curve of Reimer et al. (2013).

5. Results

5.1. Terrace mapping and terrace profiles

A total of eight Mantaro River terraces was mapped (Figs. 4 and 5) with T1 at 2 m above (+) the floodplain (FP), T2 at 4 m + FP; T3 at 7 m + FP; T4 at 26 + FP; T5 at 58 + FP; T6 at 123 + FP; T7 at 140 + FP and T8 at 183 + FP (see Transect A-A´ in Fig. 5). The contact between the oldest terrace and the basin border is located at 200 m above the current floodplain. The terraces form flat, continuous surfaces in the valley and are up to four kilometres wide. The surfaces of the older terraces (T7 and T8) have steeper gradients when compared to the younger terraces (Fig. 5). The terrace scarps may be up to 60 m high. The terraces are almost exclusively located west of the Mantaro River with the oldest terrace located almost 13 km west of the Mantaro River. In terrace levels T5 to T8 up-to 50-m-high folds have formed that strike parallel to the Mantaro basin limit. These folds have open, almost cylindrical shapes and some outcrops, especially the ones close to the basin border, show that the folds deform the basin fill.

In the Cunas River valley seven main terrace levels were identified. T1 is located at 1–2 m + FP; T2 at 2–4 m + FP; T3 at 7–8 m + FP; T4 at 12–13 m + FP; T5 at 14–18 m + FP; T6 at 22–25 m + FP and T7 at 31–34 m + FP (Fig. 4). For the sake of simplicity and clarity, we only present terrace map data from the area surrounding transect B-B´ (downstream end) and from transect C-C´ (upstream end). The terrace surfaces are up to 500 m wide on the downstream end (see Figs. 6 and 7) and decrease in size going upstream (Figs. 8 and 9), where they may be as little as 10 m wide. Terraces are located on both sides of the river valley. The terrace levels are regularly spaced with 5-m vertical intervals between them and are located up-to 34 m above the current floodplain. The reconstructed terrace profiles show that the terrace threads run parallel to each other and to the current river floodplain (Fig. 10). The T7 from the Cunas River grades into the T5 Mantaro River terrace, suggesting that the T5 from the Mantaro River acted as the main base-level in which the Cunas system started to incise. Similarly, the T3 Cunas level grades into the T3 Mantaro terrace, and the T2 Cunas level into the T1 Mantaro level, suggesting that those river terraces formed at the same time (Table 1). For a detailed discussion on the ages we refer to paragraph 5.5.

Throughout the Cunas River valley, we found small terrace levels of local extent. Because of the fragmented and irregular nature of these terraces, as well as the measurement error of the altimeter of the GPS (2–4 m), we grouped them into the main terrace levels. In the upstream section however, we discovered a complete series of fluvial terraces. Here, we mapped a total of 11, generally 20-m-wide, terrace levels with the vertical distance between the terraces being approximately 2 m (Figs. 8 and 9).

5.2. Sedimentology and stratigraphy

Stratigraphical descriptions were made throughout the study area, but here we present the data from three representative areas: one for the Mantaro River valley (in the vicinity of transect A-A´) and two for the Cunas River valley (Transects B-B´ and C-C).

5.2.1. Terraces of the Mantaro River (Transect A-A´)

In the Mantaro valley three different kinds of stratigraphical successions were found:

i) Fluvio-lacustrine deposits dominated by a fine-grained facies (Terrace T5);
ii) Fluvial deposits dominated by a gravel facies (Terrace T4); and
iii) Fluvial deposits with an even distribution of gravel and fine-grained facies (Terraces T3 and T2).

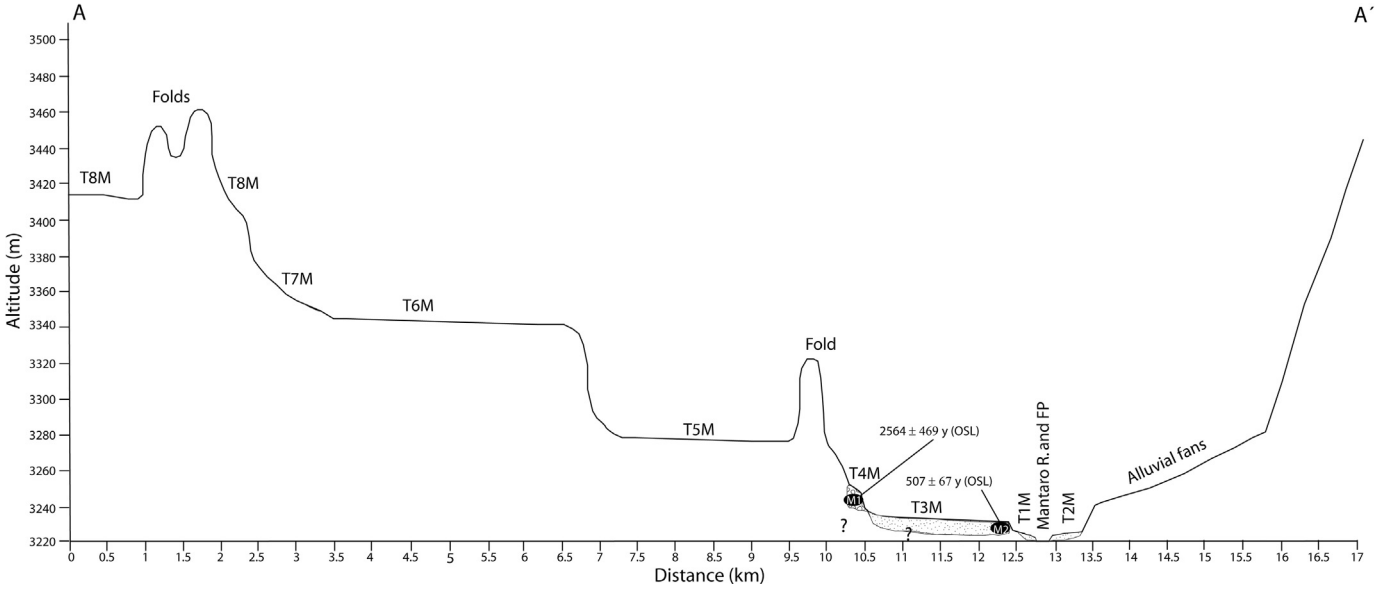

Fig. 5. Cross-section A-A´ of the Mantaro valley and its fluvial terrace sequence. For location cross-section see Fig. 4.

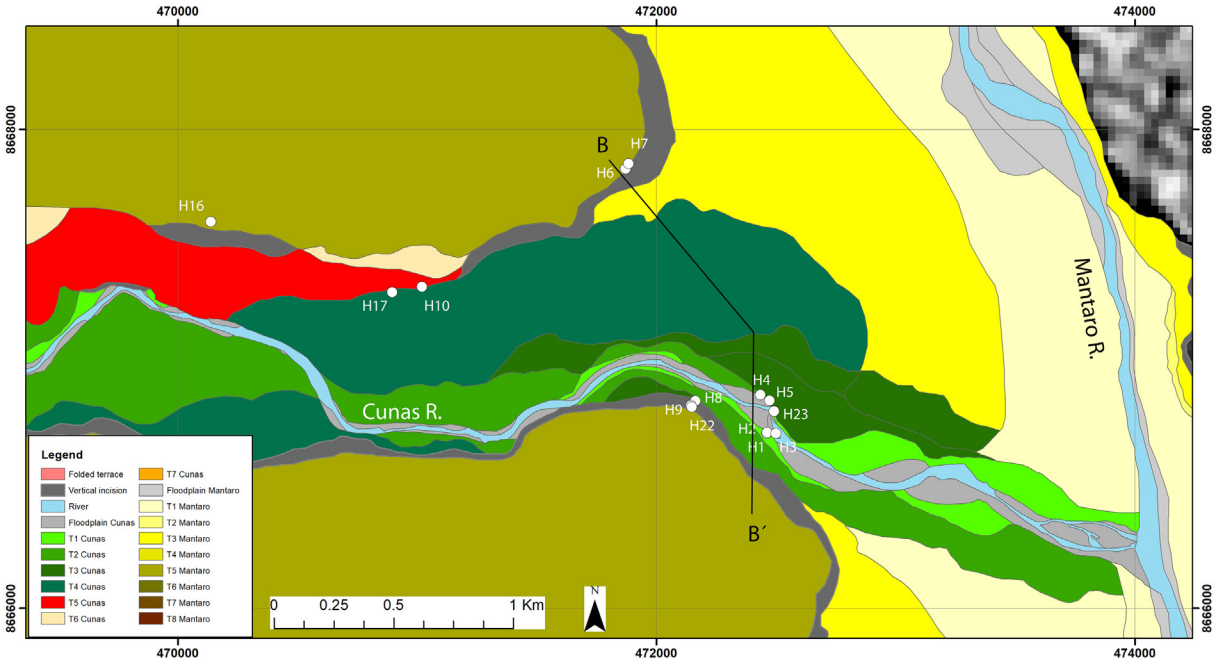

Fig. 6. Map of fluvial terraces of the Cunas River on the downstream end of the valley. Here the terraces merge with the Mantaro River terraces. Numbers H1 to H22 refer to locations of the OSL and ^{14}C samples.

The fine-grained facies, which geomorphologically corresponds to the Mantaro T5 terrace, is best exposed there where it is cut by the Cunas River. For that reason this succession is described in the section detailing the terraces of transect B-B´ located in the Cunas River valley.

5.2.1.1. Lithofacies description T4. Terrace T4 consists of least 15 m of predominantly rounded to subrounded gravels in a clast-supported matrix of medium-grained, grey sand (lithofacies *Gt;* see Fig. 11a and Table 2). The gravels are moderately sorted with medial clast sizes of seven to ten centimetres. Cobbles and boulders are not present. Clast imbrication is towards the south and in line with the current flow direction of the Mantaro River. The gravels are organised in normal graded, stacked channels of approximately 60 cm deep and up to 3 m wide that cut underlying and juxta positioned channels. Individual channels may be separated by 25 cm-thick and 2 m-wide lenses of medium-to fine-grained and horizontally-stratified sands representing channel fills (lithofacies *Sh*). Rip-up clasts of silt and clay fractions sometimes line the base of the gravel channels. The flow regime indicates a non-viscous, turbulent fluid flow (Miall, 1996). We interpret the stratigraphical succession as belonging to a shallow, gravel-bed braided river (c.f. Miall, 1996). This is inferred on the basis of the erosional, shallow, stacked channels where gravels dominate as well as the presence of rip-up clasts.

5.2.1.2. Lithofacies description T3 and T2. The base of the stratigraphical succession is made up of an at least 3-m-thick sequence of gravels and sands (Fig. 11b). The gravels are arranged in 10-cm-thick and up-to 2.5-m wide, horizontal sheets that wedge out at both ends (lithofacies *Gh*; see Table 2). Medial gravel sizes in the sheets are around 2 cm. The largest clast measure up to 5 cm. The gravels are clast-supported in a matrix of mud-sized material. They are rounded to subrounded and lacking a clearly developed imbrication. The gavel sheets alternate with tabular, also 10 cm-thick and up-to 2 m wide sheets of moderately-sorted, fine sands and silts with a reddish hue (lithofacies *Fsm*; Table 2). Sedimentary structures are absent in both sand and gravel sheets.

The top of the stratigraphical succession is made up of approximately 2 m of fine sandy, silty and clayey deposits with a reddish hue (lithofacies *Fsm*). The facies is massive without any discernible stratification, laminations or sedimentary structures except there were the clay fraction is more present and drying of the clays led to horizontal partitioning along the faces of the clay minerals. Locally, the top portion may be incised by a small channel of < 0.5 m deep and 0.5 m wide with a gravel lag at the base and fine sandy material in the top.

The T2 terrace was only partly exposed. The limited outcrops available show that the exposed part is made up of the same lithofacies *Fsm* as described for the T3 terrace.

Facies *Gh* and the interbedding facies *Fsm* together are interpreted as channel lags and fills in a medium-energy fluvial environment with a turbulent-laminar flow regime. The overlying facies *Fsm* is interpreted as overbank deposits from a medium-energy, non-cohesive floodplain typical for unconfined valleys (c.f. Nanson and Croke, 1992). Based on the above, the entire facies association is interpreted as belonging to a gravel-sand meandering river system (Miall, 1996).

5.2.2. Terraces of the Cunas iver downstream end (Transect B-B´)

5.2.2.1. Lithofacies description. The entire stratigraphical succession is exposed from the Cunas River up to the valley rim (Fig. 12). At this site, the valley rim constitutes what we geomorphologically mapped as the T5 Mantaro-T7 Cunas terrace intersection (Fig. 4). The base of the section consists of two metres of moderately-sorted, grey, coarse to medium-grained, massive sands without any discernible sedimentary structures (lithofacies *Sm*; see Table 2). From 2 m to 4.0 m, 10-cm-thick beds of grey, fine-grained sands alternate with 5-cm-thick beds of reddish very fine sand and silt. In the lowermost sands, foresets are visible which are dipping towards the south (Lithofacies *Sp*). In some of the foresets gravels with median sizes of 0.5 cm are present and maximum sizes of 1 cm. In the very fine sands and silts wave ripple structures are discernible (lithofacies *Fl*). From 4.0 to 4.5 m the fine-grained and medium-grained couples attain both 5-cm thicknesses. From 4.5 to 5 m, grey-reddish clays containing varves are present (lithofacies *Fc*). From 5 to 7 m medium-grained, red sands were deposited without any discernible structures (facies *Sm*), followed by a thick sequence of weakly laminated, reddish fine sands and silts (facies *Fl*) that continue until 17 m. From 17 to 19.5 m, 30-cm-thick, horizontal beds of reddish-grey, stratified very coarse sands (facies *Sh*;

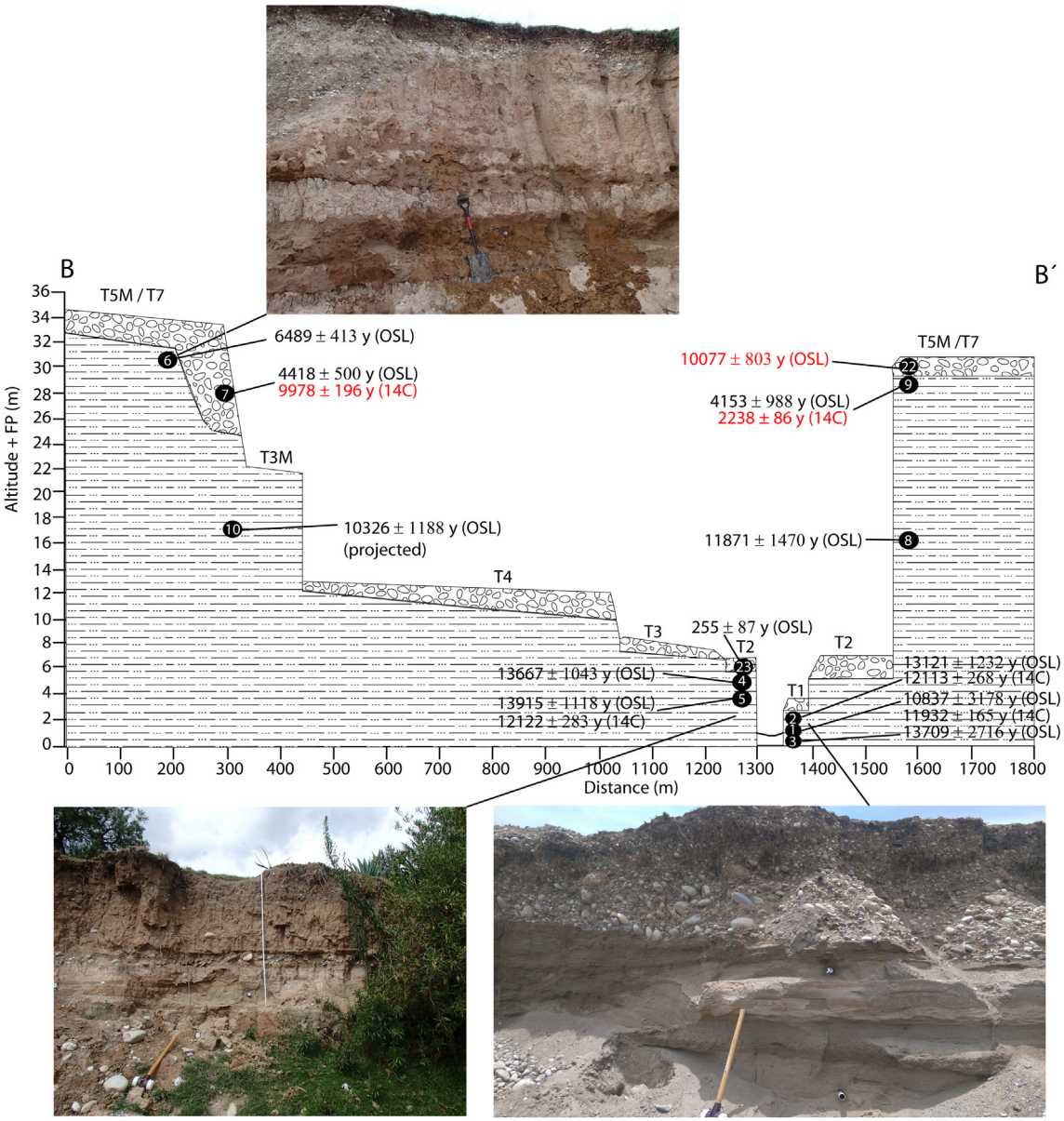

Fig. 7. Valley cross-section B-B´ of the downstream end of the Cunas River valley. For location of cross-section see Fig. 6. Numbers 1 to 22 refer to locations of the OSL and ^{14}C samples. In red the rejected ages. (For interpretation of the references to colour in this figure legend, the reader is referred to the web version of this article.)

Table 2) are alternating with 10-cm-thick beds of fine sands and muds (facies *Sm*), which culminate in a one-metre thick clay layer (Fig. 12). Weakly laminated, reddish fine sands and silts continue up to 27 m (facies *Fl*; Table 2) followed by a one-metre thick stack of pebbles in a clast-supported matrix of medium to coarse sands. The pebbles have sizes of up to 6 cm and show a weak imbrication towards the southeast. The pebbles are organised in weakly developed planar crossbeds (facies *Gp*; Table 2). After that, a fining upward sequence occurs of medium sands to silts and clays (*Fl*). At 29.5 m the sand-silt sequence is cut by a well-developed channel which is filled in with a coarsening-upward sequence of 1.2 m-thick, coarse, crudely stratified sands that grade into granules (lithofacies *Ss*). At the base of the channel a small gravel lag is found. The granules are topped by a 0.6 m-thick bed of subrounded boulders that grade into a 2 m-thick succession of rounded to well-rounded cobbles and then gravels (lithofacies *Gp*). The gravels are clast-supported with a greyish, coarse-sandy matrix and with clearly developed imbrications towards the east. The sequence ends with a 0.5 m-thick, clay bank (facies *Fc*). The overall aspect of the entire sequence is that of inverse graded and then back to normal graded sediments (Fig. 12).

The other terraces in this area have a very similar stratigraphy: always reddish fine sands and silts at the base (generally facies *Fl*) with on top maximally an 8-m-thick stack of lithofacies association *Gp* and *Fc*. The contact between *Fl* and *Gp* is always erosive.

The facies association between 0 m and 4.5 m shows a fluvial sequence that transforms in a lacustrine environment as evidenced by the fining upward sequence and lacustrine structures such as wave ripples and varves in the top part. From 4.5 m until 29.5 m the section appears to be fully lacustrine. Evidence shows massive fine to very fine sands with weakly stratified, horizontal laminations and clays with varves. In some places current structures are visible, such as planar beds as well as local incursions of coarse sandy material. The amount of sediments (at least 34 m) is considerable and would need a deep water environment to accumulate. We therefore tentatively interpret this sequence as a lacustrine environment with presence of waves and currents. The section between 28 m and 30 m contains a first fluvial incursion as shown

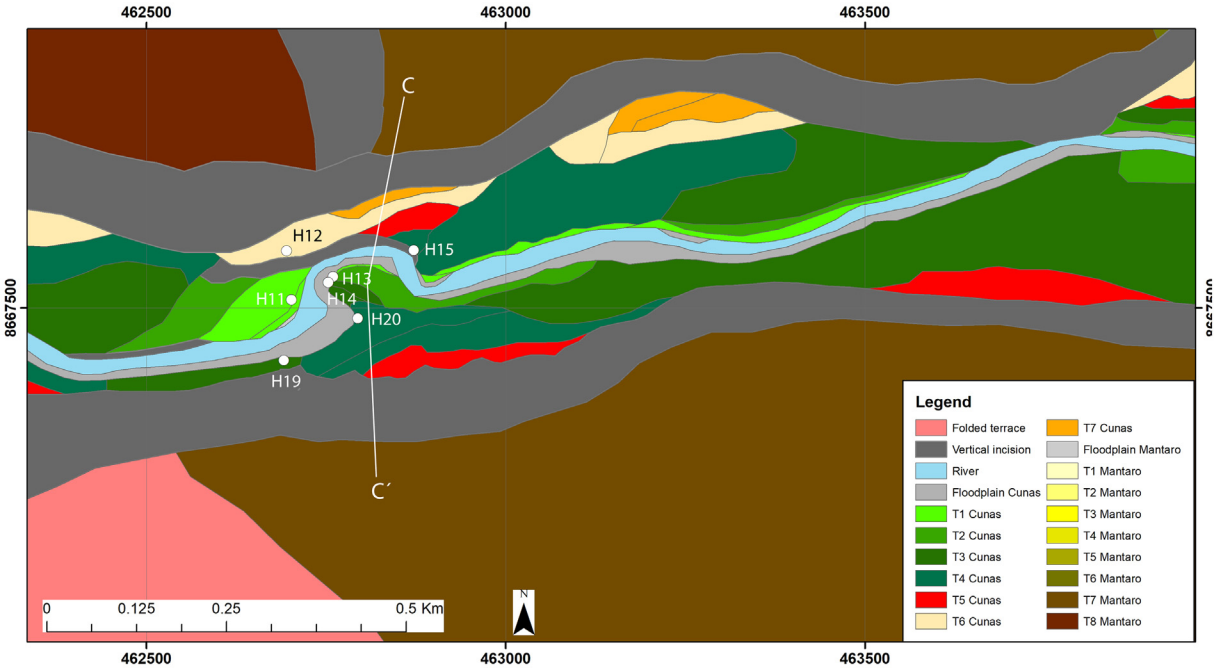

Fig. 8. Map of the terraces of the Cunas River on the upstream end of the valley. Numbers H11 to H19 refer to locations of the OSL and ^{14}C samples.

by the gravel bed that grades into finer material. This sequence is followed by a much more developed second fluvial phase that cut into the overbank deposits of the first fluvial phase (30 to 32 m) and developed a clear, single channel structure. The channel fill shows a sequence of inverse grading and then back to normal grading. This suggest an initial hyperconcentrated, dispersive water flow which then grades into a turbulent water flow (cf. Miall, 1996). The overlying facies *Fc* is interpreted as overbank deposits of a high-energy, non-cohesive and confined floodplain (Nanson and Croke, 1992). The entire facies association between 28 and 32 m is interpreted as a high-energy, gravel-bed meandering river system with limited floodplain development (cf. Miall, 1996).

5.2.3. Terraces of the Cunas River upstream end (Transect C-C´)

5.2.3.1. Lithofacies description T6, T4B and T3C. All terrace outcrops studied have at the base a fabric of ill-defined, horizontally stratified coarsening-upward sequences of medium sand that grade into coarse sand, granules and finally rounded to subrounded pebbles (Fig. 13a; Table 2). The contact between the sequences is generally abrupt but not erosive. The sequences are between 0.5 m and 3 m thick and generally matrix-supported. The matrix consists of muds, silts and fine sands. Maximum diameter of the pebbles is 10 cm, and the medial size is around 5 cm. Imbrication is not present. Limestones and volcanic rocks dominate. This facies may be almost 100 m thick as shown in the exposed valley wall and is folded close to the basin border (lithofacies *Gmg;* Fig. 13a and Table 2). This facies occurs in the midstream and upstream parts of the Cunas valley, where the river cuts the T6 and older Mantaro river terraces. They correspond to the Pliocene "Chupaca gravels" of Wise, 2007; (Fig. 3).

Lying unconformably on top of facies *Gmg*, an up-to 5 m thick sequence of clast-supported gravels is found. The majority of the clasts have a diameter of around 10 cm with the largest clast up to 30 cm in diameter. Clasts are generally rounded and show a well-developed imbrication towards the east. Up-to one metre-thick, crudely developed planar crossbeds are present in the gravels and this facies is therefore designated *Gp*. Individual stacks of narrow channels are not visible (Fig. 13a).

The upper part of the stratigraphical section consists of a succession of up-to 2-m-thick, fine sands and silts (lithofacies *Fl*). Ten-cm-thick, weakly developed, planar crossbeds containing gravel strings with clast diameters of up-to 2-cm in diameter may be present. The oblate gravels are imbricated along the planar beds. The planar beds wedge out against one another with opposite-dipping directions. A brown Ah-horizon formed in this fine sequence making it difficult to discern any other sedimentary structures or laminations that may be present in the fine fraction.

The massive character of facies *Gmg* and couplets of horizontally matrix-supported coarsening upward gravels indicate a regime of hyperconcentrated flows alternating with sheet-like fluid flows. The absence of erosional surfaces and a clearly developed channel morphology preclude a purely fluvial (e.g. braided river) environment. This is also corroborated by the fact that facies *Gmg* is only found close at the western margin of the Huancayo basin but not farther downstream the Cunas valley. We therefore conclude that lithofacies has a limited spatial extent. Considering all the evidence presented, we interpret lithofacies *Gmg* as belonging to a sheet flood fan (c.f. Nichols, 2009) and not as as sediments from the Mantaro River as proposed by Wise (2007).

Facies *Gp* shows the presence of a channel morphology and clearly imbricated clasts under a regimen of a hyperconcentrated flow. We therefore interpret it as a fluvial channel fill or a gravel bar. Facies *Fl* is shows overbank fines with occasional incursions of a weakly developed fluvial current depositing small gravels. We interpret this facies as a high-energy, non-cohesive floodplain typical for areas with steep terrain where lateral migration of the channel is limited due to confinement by the narrow river valley (c.f. Nanson and Croke, 1992).

Considering the above, we interpret the facies association *Gp* and *Fl* as a gravel bed meandering river system (c.f. Miall, 1996).

5.2.3.2. Lithofacies description T5, T4A to T1A. The base of the terrace deposits is made up of the same facies *Gmg* as described in the foregoing section. Lying unconformable on top of this facies are rounded to subrounded pebbles and boulders with diameters of up to 60 cm (litofacies *Gp;* Fig. 13b) followed by very coarse, weakly stratified sand with 5-cm large, rounded to subrounded pebbles (lithofacies *Sp*; Table 2). The entire suite is approximately one to two metres thick and forms lateral accretion surfaces dipping 30° towards the current river bed. The facies has a greyish tone to it and shows very little signs of

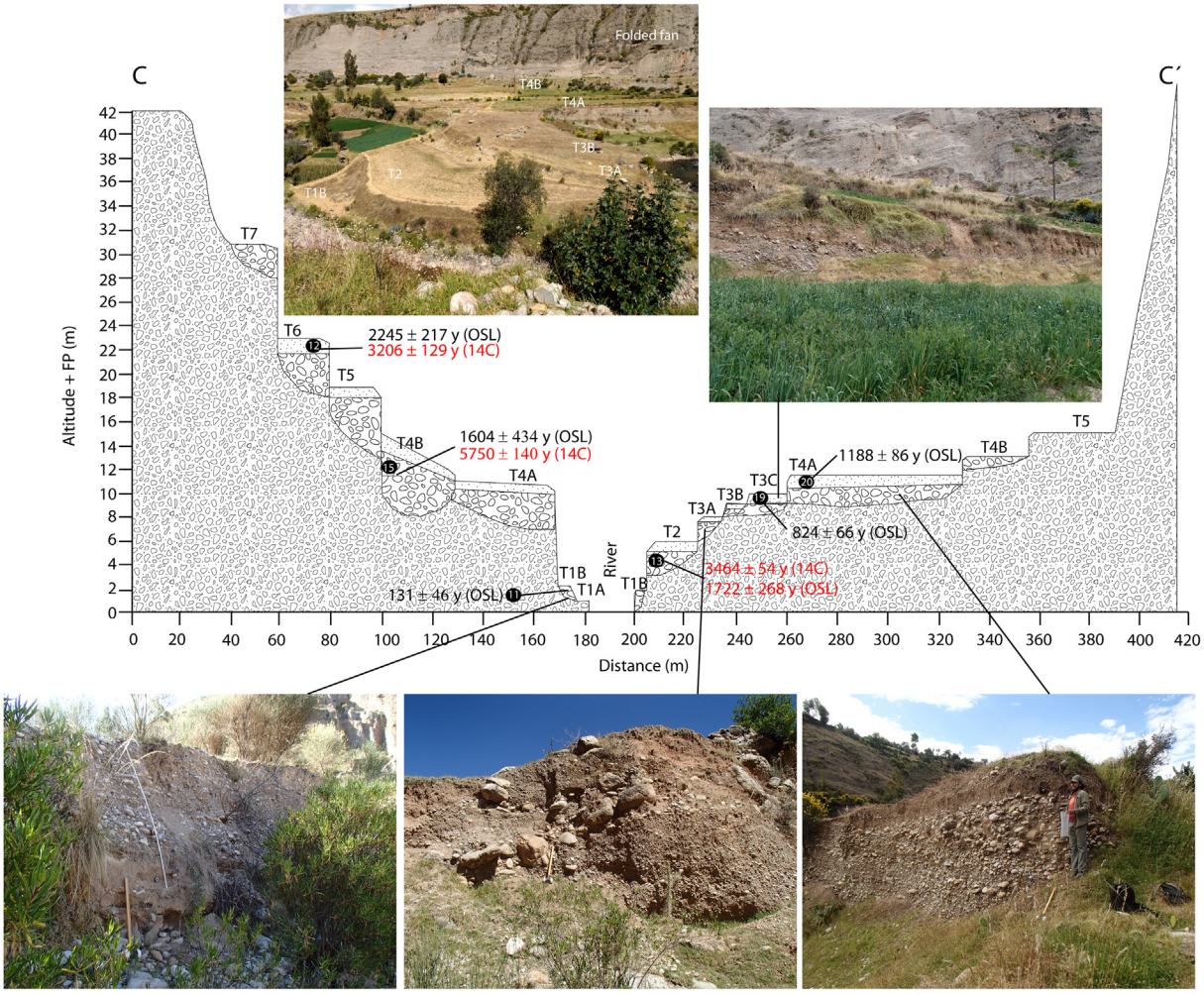

Fig. 9. Vally cross-section C-C´. At this location a sequence of 11 terraces was recognised and mapped in detail. Subdivisions of major terrace levels T1 to T7 are marked with letters A,B and C. Numbers 11 to 20 refer to locations of OSL and ^{14}C samples. In red the rejected ages. (For interpretation of the references to colour in this figure legend, the reader is referred to the web version of this article.)

weathering. On top of the series of lateral accretion surfaces there is a metre of fine sands and silts with strings of small pebbles, identical to lithofacies *Fl* as discussed in the foregoing section.

Lithofacies *Gmg* was interpreted as a sheet flood fan as discussed in the former paragraph. Facies *Gp* and *Sp* are interpreted as a channel lag of an actively migrating meander. Facies *Fl* is interpreted as overbank deposits of an active floodplain with occasional incursions of fluvial currents. Facies association *GP, Sp* and Fl are interpreted as a gravel bed meandering river system as evidenced by the lateral accretion surfaces and the preserved meander forms (Fig. 13b).

5.3. Differentiating between the Cunas terrace sediments and older sediments

On the basis of the sedimentological and stratigraphical evidence presented above we can distinguish different depositional environments. In the downstream part of the Cunas valley (transect B-B´) reddish, lacustrine fine sediments are incised by a gravel-bed meandering river system with limited floodplain development which flowed towards the east (facies association *Gp* and *Fl*). In the upstream section of the Cunas River (transect C-C´), matrix-supported gravels which we interpret as sheet flood fan deposits, are also incised by the same type of gravel-bed meandering river system with the same facies association and same flow direction. Geomorphologically, the various terrace surfaces formed in those deposits can also be correlated throughout the Cunas River valley (Fig. 10). Based on these observations, we suggest that the upper facies association *Gp-Fl* belongs to the Cunas River terraces.

All the investigated terraces belong to the cut-fill-cut type (Bridgland and Westaway, 2008a), whereby the first stage of terrace formation is dominated by vertical incision in the underlying, older sediments and lateral erosion of the valley walls. The horizontally extensive packages of sediment as well as the lateral accretion surfaces of the meanders shows that the newly created space is filled up with sediments. In the case of the Cunas terraces, up-to 7-m thick accretional packages were formed and in the case of the Mantaro River they may be as much as 15 m thick (T4 terrace) and possibly more. The final stage of terrace formation is that of renewed vertical incision whereby a terrace scarp is formed. Field evidence shows that the vertical incision extends below the base of the terrace deposit and incises into the older, underlying sediments (Figs. 7 and 12).

5.4. OSL analysis

5.4.1. Annual dose-rate

Of the 25 samples collected, 22 samples were dated. The gamma spectrometry of the samples showed similar results for ^{238}U, ^{235}U and ^{232}Th series and for ^{40}K activity (Table 3). ^{235}U activity concentration is below detection limits and no disequilibrium is observed in ^{232}Th and ^{238}U decay chains for most samples. Disequilibrium in ^{238}U was only

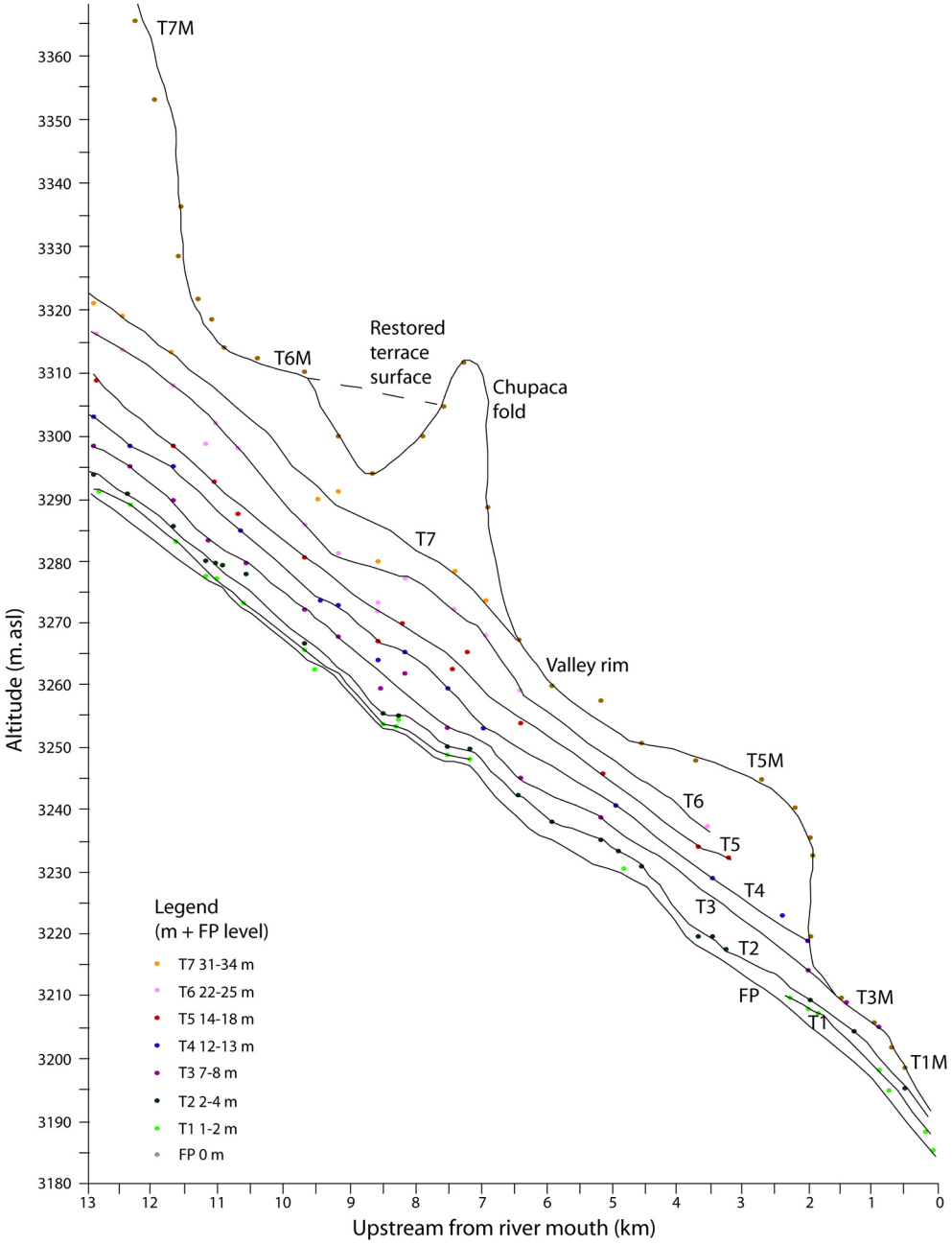

Fig. 10. Longitudinal terrace profiles of the Cunas T1 to T7 terraces. The valley rim is made up of (folded) Mantaro river terraces T1 to T5 that were incised by the Cunas River.

Table 1
Correlation between the Cunas and Mantaro River terraces based on altitude above their respective floodplains (m + FP).

Cunas		Mantaro	
Terrace	m + FP	Terrace	m + FP
T7	31–34	T5M	31–34
T6	22–25	T4M	26
T3	7–8	T3M	7
T2	2–4	T1M	2

observed in some of the lake sediments (Fig. 12). This provides differences in the estimated D_r of 2%–5%, except for sample H1 which shows a difference of 10%. Thus, such disequilibrium has a negligible effect on the calculated dose rate and differences are within the limits of measure uncertainties except for sample H1. So, equilibrium was assumed until the present day, including sample H1 because samples above and below (H2 and H3) do not show disequilibrium and its age will be constrained by the ages of these samples.

Saturation values were very variable ranging from 16% to 44%, and around 25% to 30% for most samples. For the older lacustrine samples, saturation was assumed until the deposition of the overlying fluvial sediments thereby considering it constitutes an average value between saturation and dryness values. For the younger fluvial sediments an average value between saturated and dry states was used.

A similar assumption was used to assess the cosmic dose rate (D_c) for the lowermost, and presumably older, lake samples as there have been changes in the D_c due to burial by continuous sedimentation until the onset of fluvial incision.

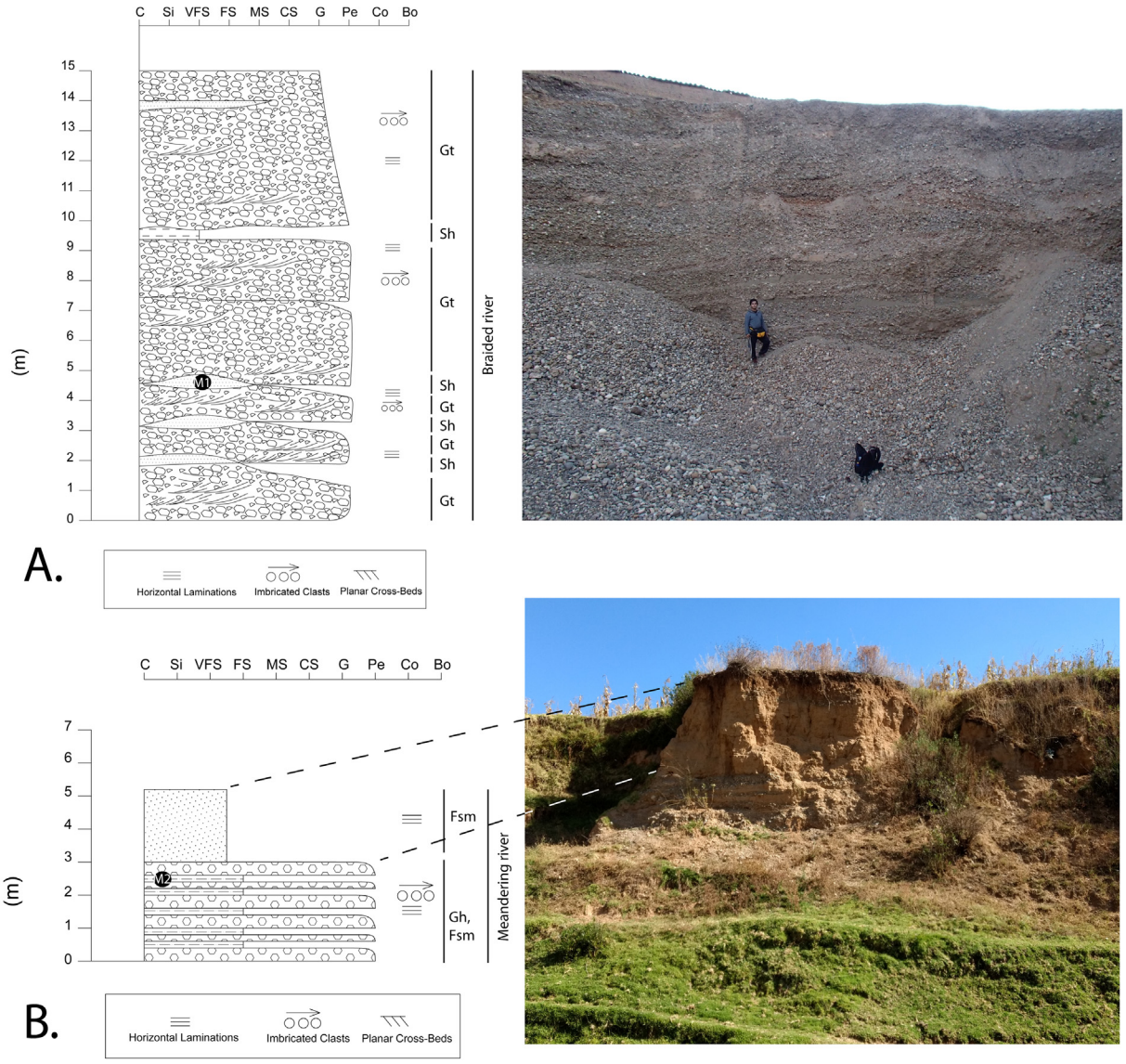

Fig. 11. Stratigraphical columns of the sections discussed for Transect A-A´. Numbers M1 and M2 refer to OSL samples. For stratigraphical codes see Table 1.

5.4.2. Equivalent doses

The OSL measurements showed dim but fast signals. After performing preheat tests we used 220 °C preheat temperatures for samples H2, H3, H4, H5 and H10, and 240 °C temperatures for samples H1, H9, H17 and M2. For the other samples a 200 °C preheat temperature was used. A large number of aliquots were measured for all samples, as the dim signals provided rejection of most of them. For some samples a set of aliquots with 100 grains was compared with a set of aliquots of 10–20 grains. This has been helpful in identifying partial bleaching. The distribution of such aliquots was compared for the oldest samples H1 to H5 which provided the brightest signals. Aliquots of 100 grains provided less asymmetric distributions but higher D_es, due to the measurement of mixed signals from partially and fully bleached quartz (Fig. 14). Small aliquots provided asymmetric distributions for most samples, except for H12, H19 and H20 (Fig. 14). The overdispersion of the mean (Galbraith et al., 1999) was very high indicating partial bleaching except for samples H19 and H20. Other possible causes of this overdispersion are beta microdosimetry (Mayya et al., 2006) and the poor signal-to-noise ratio in the youngest samples (Ballarini et al., 2003; Madsen and Murray, 2009). This was not observed in samples H19 and H20. Dose recovery tests provided ratios within 1.0 ± 0.1 for all samples, but overdispersion values were still relatively high (≥20%) for samples H5, H7, H19, H16 and H19. Thus, a sum of partial bleaching, beta microsdosimetry and poor signal-to-noise ratio are the probable causes of the high overdispersion. Thus, the Minimum Age Model (MAM, Galbraith et al., 1999) was used to estimate most ages (Table 4). The Central Age Model (CAM) was used for samples H12, H19 and H20, as negligible incomplete bleaching of the residual signal before burial was observed for the overdispersion and observed D_es distributions.

5.5. Radiocarbon and OSL dating results

The OSL ages range from 49,009 ± 16,966 years ago to 131 ± 46 years ago (Table 5) and the radiocarbon ages from 12,122 ± 283 years BP to 2238 ± 86 years BP (Table 6). To compare them with published paleoclimate data, OSL ages are provided in years before the year 2018; ^{14}C ages are at 2σ confidence interval and in years before 1950 (Table 6). The Mantaro terraces T3 and T4 of transect A-A´ have chronologically consistent ages of 507 ± 67 years ago (sample M2) and 2564 ± 469 years ago (sample M1; Fig. 11).

OSL and ^{14}C ages for the sediments in transect B-B´ are largely consistent between them and also stratigraphically (Fig. 7). For the OSL ages, there is a general decrease in age for the lacustrine deposits from

Table 2
Facies codes of Miall (1996) and interpreted depositional environments on basis of sedimentology and stratigraphy.

Lithofacies (Miall, 1996)	Description	Sedimentary and erosive structures	Interpretation	Part of depositional environment (this paper)
Gmg	Graded, matrix-supported gravel	Graded	Debris flow deposit	Fan
Gt	Clast-supported gravel	Through-cross bedding	Channel fill	Gravel-bed braided river
Gp	Clast-supported gravel	Planar cross-bedding	Channel fill	Gravel-sand meandering river system
Gh	Clast-supported gravel with horizontal stratifications	Weak horizontal stratification; imbrication	Channel fill; bar	Gravel-sand meandering river system
Sm	Very fine to very coarse massive sand	Absent	Channel fill, lacustrine	Gravel-sand meandering river system
Sp	Very fine to very coarse sand	Planar cross-bedding	Channel fill	Gravel-sand meandering river system
St	Fine to very coarse sand	Through-cross bedding with gravel lag	Channel fill	Gravel-sand meandering river system
Sh	Very fine to medium sand	Horizontal bedding with laminations	Crevasse splay; subaquaceous fan	Proximal floodplain; lake border
Ss	Coarse to very coarse, poorly sorted sand	Incised channel with sand or gravel lag	Channel fill	Gravel-sand meandering river system
Fc	Clay	Varves	Lake	Deeper part of lake
Fsm	Silt and clay	Absent	Distal floodplain, lacustrine	Gravel-sand meandering river system
Fl	Very fine sand, silt and mud	Interbedded, possibly graded laminations	Floodplain or shallow lake, proximal to channel	Gravel-sand meandering river system; lake

13,709 ± 2716 years ago for the lowermost sample (H3) to 6489 ± 413 years ago for the uppermost sample H6. Ages of samples H2 to H10, excluding H7, follow this stratigraphical trend. The overlying deposits of the Cunas T7 terrace on the north bank were OSL-dated at 4418 ± 500 years ago (H7) and ^{14}C-dated at 9978 ± 196 years BP (sample H7). The OSL age corresponds well with the OSL-age of sample H9 (4153 ± 988 years ago), which was taken from the T7 Cunas terrace on the south side of the valley. The ^{14}C age of H9 presents a lower age of 2238 ± 86 years BP. The reasons why we think the ^{14}C underestimates the OSL age are explained further down below, together with the ^{14}C ages of transect C-C´. In the remainder of this paper we will use the age of sample H7 as representative for the T7 terrace as it has a smaller error when compared to the one of sample H9. Finally, the OSL age of 10,077 ± 803 years ago for the uppermost sample H22 is not consistent with the stratigraphical sequence and overestimates the real age due to incomplete bleaching of the geological signal of quartz grains (Tables 4 and 5). The age of 255 ± 87 years ago for sample H23 corresponds to a sample taken from sediments that belong to terrace T2 of the Cunas River. This age is younger than the one of terrace T7 (sample H7) and therefore stratigraphically consistent.

The samples of transect C-C´ were all taken in sediments that according to our stratigraphical interpretation belong to sediments of the Cunas River terraces (facies G*p* and S*p* in case of all samples; sample H12 was taken in facies *Fl*). The OSL ages increase with increasing terrace elevation from 131 ± 46 years ago (sample H11) to 2245 ± 217 years ago (H12) and are therefore stratigraphically consistent (Fig. 9). Only sample H13 overestimates the age due to partial bleaching of the geological signal of quartz grains (Tables 4 and 5).

The^{14}C ages of the samples are much older than the OSL ages in this section and chronologically not consistent with the fluvial terrace sequence. This is most likely because the organic matter in the sediments originates from eroded soil organic matter. To verify the nature of the organic matter we used carbon stable isotope (δ^{13}C) fractioning and the C:N ratio (Table 6). The δ^{13}C for all samples (except H13) does not correspond to intact terrestrial plants, which usually range between −8‰ and − 35‰ (Deines, 1980; Wang et al., 1998), but to different biochemical components of decayed plant litter and soil microbial matter (Deines, 1980; Accoe et al., 2002; Howard et al., 2009). Both δ^{13}C and radiocarbon age of organic matter in soils increases with depth due to carbon recycling (Wang et al., 1998). Thus, the inclusion of eroded soil organic matter results in very variable δ^{13}C and radiocarbon ages and overestimates the timing of fluvial sedimentation. An exception to this is sample H9. The OSL age of H9 (4153 ± 988 years ago) is older than the calibrated radiocarbon age (2238 ± 86 years BP). Its C:N ratio fits the ratio of the overlying fluvial sediments of sample H7 (C:N ratio of ~3) and their δ^{13}C are not very different (−2.43‰ vs. +0.003‰). It is thus suggested that the dated organic matter of this sample comes from infiltration of soluble organic material from the overlying terrace sediments. In these cases, dating of the soluble fraction of the organic matter leads to underestimated radiocarbon ages (Howard et al., 2009; Ferro-Vázquez et al., 2018).

In lacustrine sediments, C:N ratios with values < 10 correspond to lacustrine algae (Meyers, 1994). The ratios of samples H1, H2 and H5 agree with this. The δ^{13}C value of H1 and H2 are also typical of freshwater algae (Deines, 1980, Wang et al., 1998), but the δ^{13}C value of sample H5 is more typical of a vegetal litter or microbial matter in soils. As the age of sample H5 agrees with that of samples H1 and H2, we think that a rapid decay process affected sample H5 shortly after deposition of the sediments. Taking the above in consideration, the data suggests that the ^{14}C ages provide the actual time of sediment deposition. This also agrees with our stratigraphical inference of a lacustrine environment and it may explain why there is an excellent correspondence between the ^{14}C and OSL ages for samples H1, H2 and H5.

Sample H16 was taken from sediments from the T7 terrace of the Cunas River, but the OSL age (6326 ± 519 years ago) is older than the

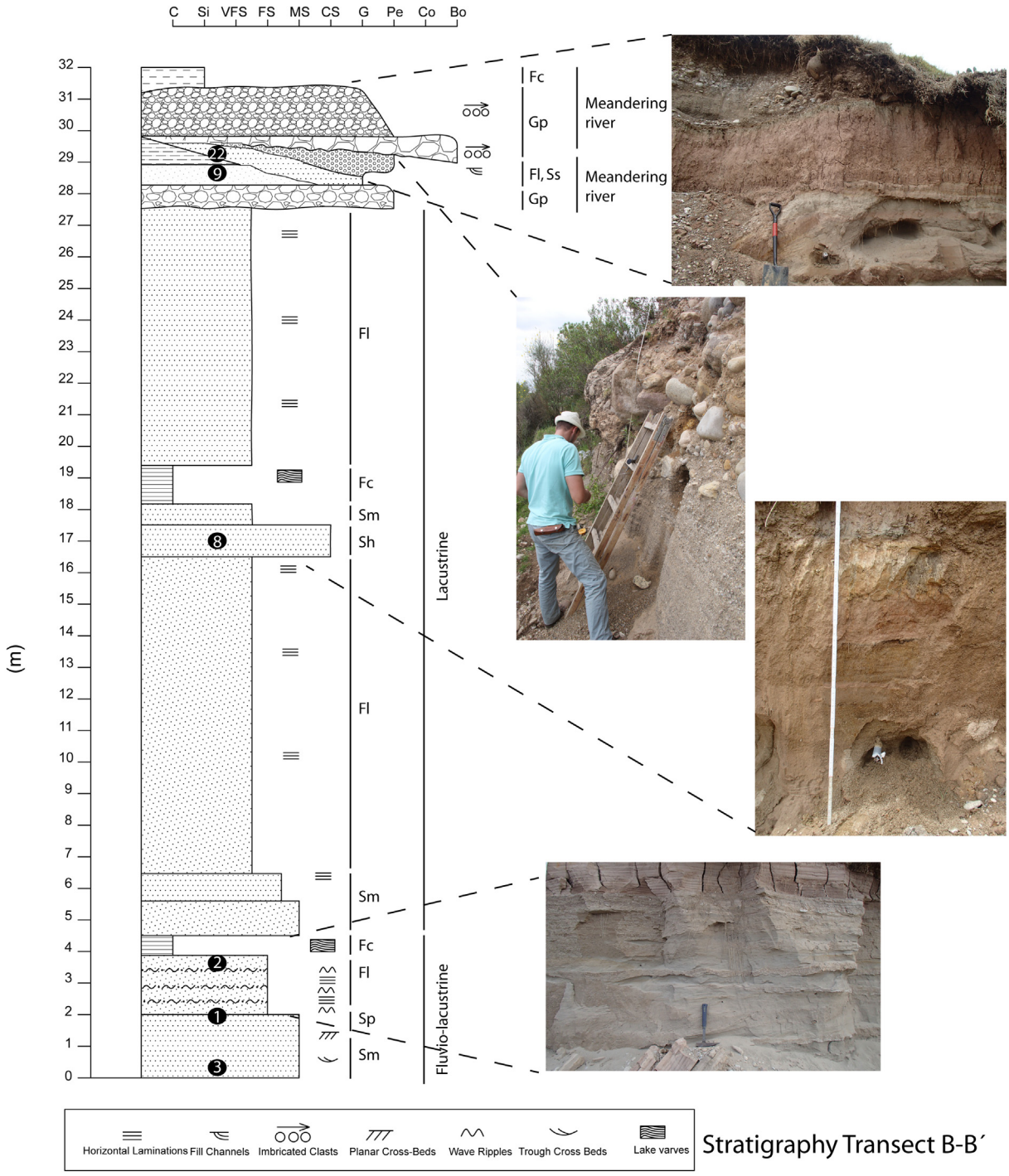

Fig. 12. Stratigraphical columns of sections discussed for Transect B-B´. Numbers refer to OSL and ^{14}C samples. For stratigraphical codes see Table 1.

ages of the same terrace further downstream (samples H7 and H9). The age and relative altitude of sample H16 however agrees well with the age of sample H6, which was taken in the topmost part of the lacustrine sediments. Perhaps the sediments belonging to H16 do not belong to the Cunas terrace. We did notice in the field that the gravels of this site were more matrix-supported and not clast-supported. So perhaps they correspond to an influx of, for instance, alluvial fan material that was deposited in the lake.

H17 shows the oldest age (49,009 ± 16,966 years ago) which is clearly overestimated due to partial bleaching (Table 5).

In conclusion, we use the OSL ages to build our chronostratigraphical model and only the ^{14}C ages of the lake deposits. The other ^{14}C ages are derived from eroded soil material and give overestimations of the depositional age. Using this approach, the ages show a consistent decrease in age from the bottom to the top of the lacustrine sediments, and the ages show a consistent increase in age with increasing terrace elevation of both the Mantaro and Cunas River terraces.

6. Discussion

6.1. Climatic controls on lacustrine and fluvial deposition

The presence of the older Mantaro terraces T6 to T8, as well as a deeply incised Cunas river valley, suggest that the Mantaro valley had

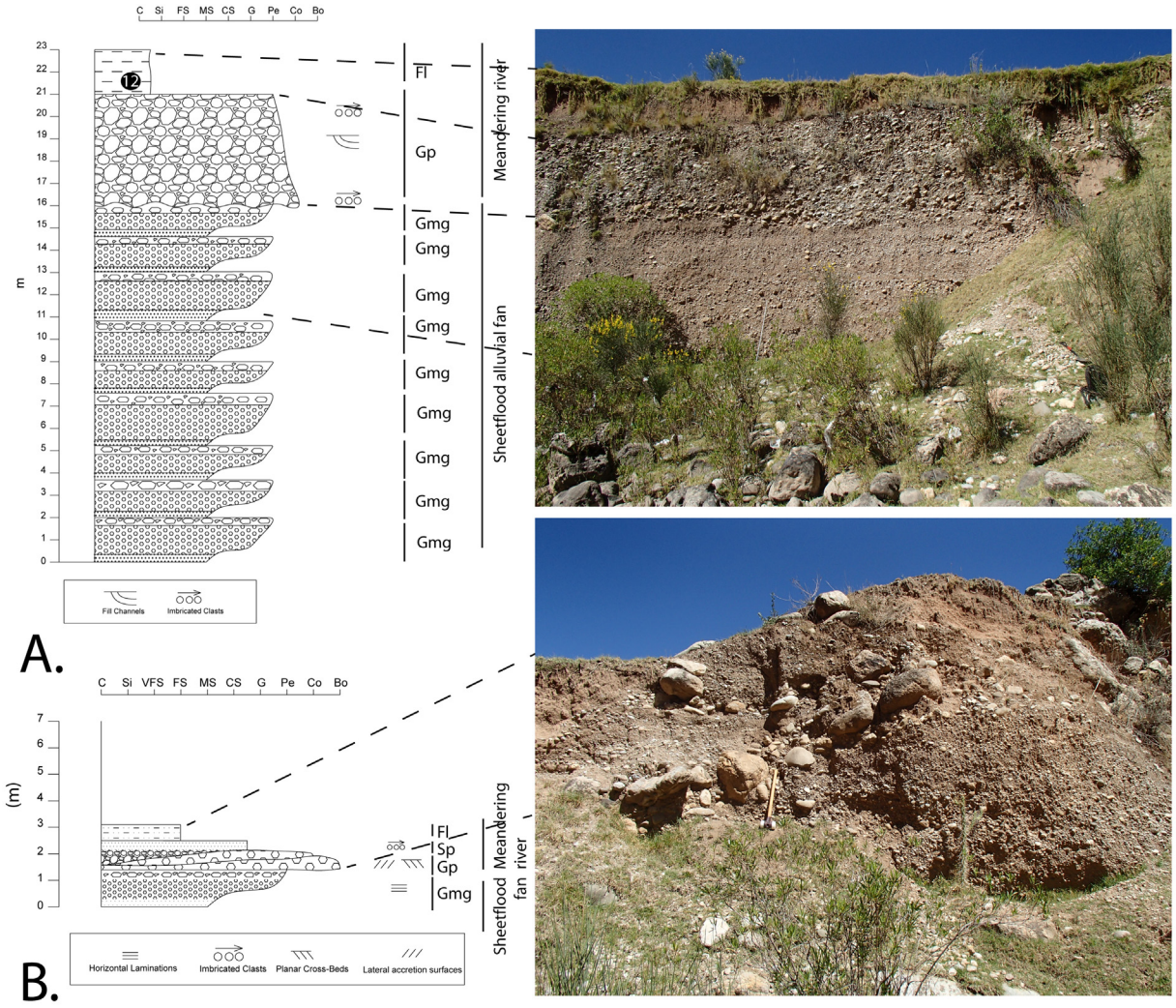

Fig. 13. Stratigraphical columns of sections discussed for Transect C-C′. Stratigraphical columns of terraces T6 and T3A are respresentative for all terraces in this transect. Number 12 refers to OSL and ^{14}C samples. For stratigraphical codes see Table 1.

Table 3
D_r OSL. Activity concentration of radionuclides measured in the samples and estimated doses: beta dose (D_β), gamma dose (D_γ), cosmic dose (D_c) and dose rate (D_r).

Sample	^{40}K (Bq Kg^{-1})	^{232}Th (Bq Kg^{-1})	^{238}U (Bq Kg^{-1})	^{214}Bi (Bq Kg^{-1})	D_β (mGy/a)	D_γ (mGy/a)	D_c (mGy/a)	D_r (mGy/a)
H1	144 ± 7	6.1 ± 0.3	8 ± 3	12.6 ± 0.7	0.32 ± 0.03	0.20 ± 0.02	0.07 ± 0.02	0.62 ± 0.04
H2	194 ± 17	8.7 ± 0.5	12 ± 3	15 ± 1	0.44 ± 0.04	0.28 ± 0.03	0.07 ± 0.02	0.83 ± 0.05
H3	167 ± 9	8 ± 1	12 ± 3	12.1 ± 0.7	0.39 ± 0.03	0.26 ± 0.03	0.06 ± 0.01	0.74 ± 0.04
H4	254 ± 13	8.3 ± 0.7	11 ± 2	13.1 ± 0.9	0.56 ± 0.03	0.30 ± 0.02	0.09 ± 0.01	0.99 ± 0.04
H5	295 ± 13	13 ± 1	14 ± 3	14.9 ± 0.6	0.69 ± 0.04	0.41 ± 0.03	0.09 ± 0.01	1.23 ± 0.05
H6	341 ± 16	15.8 ± 2.3	8.1 ± 4.1	15.6 ± 1.1	0.72 ± 0.04	0.42 ± 0.03	0.16 ± 0.03	1.49 ± 0.06
H7	206 ± 10	14.8 ± 2.1	14.5 ± 1.7	13.1 ± 1.8	0.56 ± 0.03	0.40 ± 0.03	0.10 ± 0.01	1.12 ± 0.04
H8	199 ± 9	11 ± 0.6	13.6 ± 0.8	15.4 ± 1.8	0.49 ± 0.02	0.33 ± 0.01	0.05 ± 0.01	0.89 ± 0.02
H9	218 ± 12	11.8 ± 0.7	8 ± 2	12 ± 1	0.45 ± 0.3	0.28 ± 0.02	0.12 ± 0.01	0.90 ± 0.04
H10	277 ± 19	12.2 ± 2.2	13.1 ± 8.8	16.7 ± 3.9	0.67 ± 0.08	0.40 ± 0.07	0.07 ± 0.01	1.17 ± 0.11
H11	217 ± 10	12 ± 1	11 ± 2	17.3 ± 0.8	0.52 ± 0.03	0.33 ± 0.02	0.16 ± 0.02	1.10 ± 0.04
H12	246 ± 18	24 ± 2	24 ± 5	31 ± 3	0.87 ± 0.06	0.61 ± 0.05	0.18 ± 0.03	1.73 ± 0.08
H13	241 ± 12	15.6 ± 0.7	19 ± 4	25 ± 1	0.78 ± 0.05	0.54 ± 0.04	0.18 ± 0.03	1.56 ± 0.09
H15	211 ± 11	10 ± 1	15 ± 4	16 ± 1	0.53 ± 0.04	0.34 ± 0.03	0.13 ± 0.01	1.06 ± 0.05
H16	99 ± 5	4.7 ± 0.7	5.1 ± 1.1	7.8 ± 0.6	0.27 ± 0.02	0.18 ± 0.01	0.17 ± 0.02	0.69 ± 0.03
H17	208 ± 12	10 ± 1.4	6.5 ± 2.9	17 ± 1.1	0.50 ± 0.03	0.30 ± 0.02	0.17 ± 0.02	1.05 ± 0.04
H19	383 ± 17	29.1 ± 3.6	26.1 ± 1.3	27.5 ± 1.3	0.84 ± 0.05	0.58 ± 0.04	0.21 ± 0.04	1.73 ± 0.07
H20	394 ± 8	20 ± 1	25 ± 1.3	22 ± 3	0.94 ± 0.04	0.60 ± 0.02	0.19 ± 0.04	1.82 ± 0.05
H22	204 ± 10	10.7 ± 0.6	18.1 ± 4.3	15.2 ± 0.9	0.61 ± 0.05	0.41 ± 0.04	0.18 ± 0.06	1.27 ± 0.06
H23	220 ± 15	10.7 ± 0.8	18.7 ± 5.2	18.1 ± 3.4	0.61 ± 0.05	0.40 ± 0.04	0.19 ± 0.02	1.40 ± 0.30
M1	391 ± 19	16.6 ± 0.8	20 ± 1.3	12 ± 3	0.96 ± 0.04	0.58 ± 0.2	0.10 ± 0.01	1.68 ± 0.05
M2	357 ± 18	44 ± 5	39 ± 8	44 ± 2	1.20 ± 0.05	1.02 ± 0.06	0.16 ± 0.02	2.45 ± 0.08

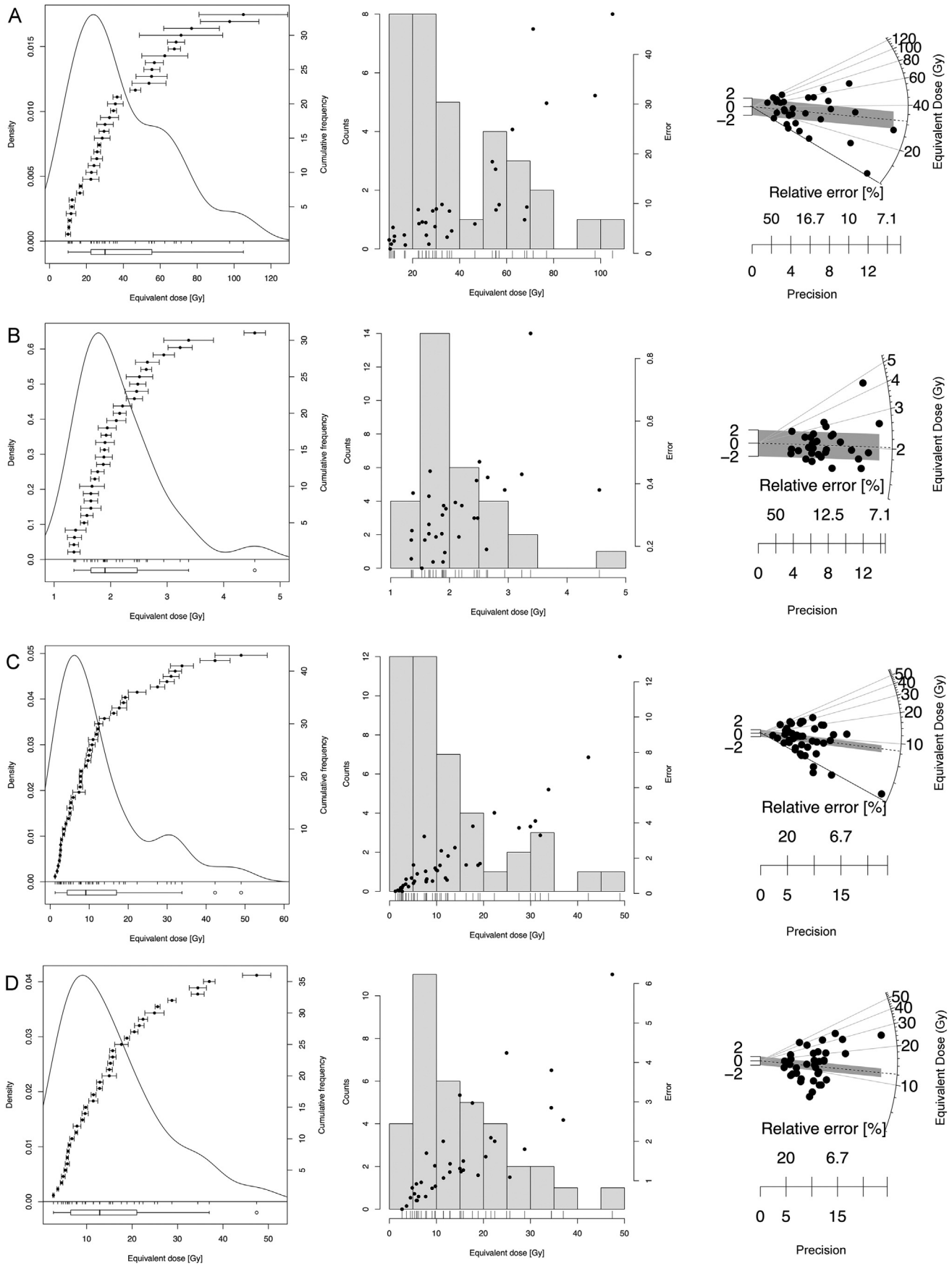

Fig. 14. D_es values of the measured aliquots for samples H2 (A), H20 (B), M2 (C) and H13 (D). The left column corresponds to kernel density estimate plots, the central column to histograms and the right column to radial plots. In radial plots, the D_e provided by the Central Age Model is shown in the grey, shaded area and the De provided by the Minimum Age Model (H2 and M2) is marked with a line. In H20 (B) this is not marked because the Central Age Model was used. In the case of H13 (D) this is because the age is overestimated with both age models due to partial bleaching.

Table 4
Results of the OSL tests performed on two different multi-aliquot sets composed of ~10–20 and ~100 grains. The equivalen dose is estimate by CAM (Central Age Model), and MAM (Minimum age model). Overdisperion (Ov) is provided and N corresponds to the number of accepted aliquots.

Sample	~10–20 grains aliquots				~100 grains aliquots			
	CAM	MAM	Ov	N	CAM	MAM	Ov	N
H1	26.6 ± 3.1	6.7 ± 1.9	57 ± 9	33	37.1 ± 2.4	6.9 ± 0.8	43 ± 5	46
H2	30.8 ± 3.5	10.9 ± 0.8	60 ± 9	33	58.5 ± 3.9	45.4 ± 4.9	10 ± 1	48
H3	29.7 ± 5.9	9.6 ± 1.2	63 ± 15	40	42.8 ± 2.6	37.5 ± 4.5	15 ± 1	42
H4	38.4 ± 5.1	13.6 ± 0.9	76 ± 10	34	108.0 ± 5.9	32.4 ± 4.1	16 ± 6	40
H5	31.9 ± 4.3	17. 1 ± 1.2	69 ± 11	34	61.7 ± 4.7	48.3 ± 5.6	15 ± 1	45

already been an exoreic basin before the formation of the Cunas and younger Mantaro terraces, as suggested by Wise (2007) and Wise and Noble (2008). Stratigraphical and chronological evidence shows that the Mantaro T5 terrace surface is formed in lacustrine sediments dated from at least 12,000 BP to shortly before 4418 ± 500 years ago, implying that the Mantaro valley was a lake until incision by the Cunas River began. As glaciers were present around the headwaters of the Mantaro and Cunas Rivers (Fig. 2), we speculate that the Mantaro valley was temporarily blocked by a glacier or glacial sediments (e.g. a moraine). Radiocarbon dating of moraine sediments in the Huaytapallana massif just northeast of the Huancayo basin shows that from 12,000 yrs. BP onwards the glaciers receded significantly and were melted completely by 8200 years BP (Seltzer and Hastorf, 1990). We hypothesise that glacial meltwater from the Huaytapallana massif may have filled the Mantaro valley and formed a lake. A profound change took place 4418 ± 500 years ago in the Huancayo basin: the lake drained, the Cunas River connected to the Mantaro River and both rivers started to incise simultaneously. This is shown by the correlation of terrace T7 of the Cunas with T5 of the Mantaro, T6 of the Cunas with T4 of the Mantaro and T3 of the Cunas with T3 of the Mantaro, based on similarities in age and elevation above their floodplains. This moment marked the initial stage of modern valley development (Fig. 10). The timing coincides with an increase in the frequency and amplitude of the SASM and with higher temperatures, as shown by numerous paleoclimatic archives of the region (Rein et al., 2005; Bird et al., 2011; Kanner et al., 2013; Schittek et al., 2015; Fig. 15). It is also a time when lake levels in the Altiplano rose (Baker et al., 2001b) and of significant retreat of the middle to late Holocene glaciers in the Peruvian Andes (Stansell et al., 2013). Glacier melt around 4000 years ago may have attributed to the onset of incision of the Cunas River valley. After this period of initial incision, some 2000 years passed in which no terrace formation was registered in the Mantaro and Cunas valleys. The majority of the terraces started to form 2245 ± 217 years ago, as shown by the OSL age of the T6 Cunas terrace (sample H12) and its counterpart, the T4 Mantaro terrace (2564 ± 469 years ago; sample M1). This timing fits very well with climate reconstructions, showing that the frequency of the SASM in the Andes suddenly intensified 2200 years BP (Seltzer et al., 2000; Rein et al., 2005; Bird et al., 2011; Kanner et al., 2013) and continued until the present (Fig. 15). In the Atacama Desert of Northern Chile, farming-based settlements flourished between 2500 and 2040 years BP, due to an increase in surface water availability, and flooding events increased drastically (Gayo et al., 2012). The intensification of high-frequency climate oscillations may also explain why the T4 Mantaro terrace was developed under braided river conditions, which are characterised by a more turbulent river flow and deposition of coarser-grained deposits. Our reconstruction also shows that the periods of fluvial sedimentation in the Cunas valley coincide with wet periods in the central Peruvian Andes, as registered in speleothem and lake records, and with periods of glacial retreat presumably due to an increase in temperature and precipitation (Fig. 15). It is also striking that no deposition took place between between 1188 ± 60 years ago and 824 ± 66 years ago (Fig. 9), which matches the drier Medieval Climate Anomaly interval (800 to 1250 years BP; Rein et al., 2004), due to subdued SASM activity (Rein et al., 2005; Vuille et al., 2012; Kanner et al., 2013; Apaéstegui et al., 2014). Stable isotopic data from Lake Umayo in southern Peru show the presence of a

Table 5
OSL ages obtained. Note: Dose rate (D_r), accepted aliquots (n), equivalent dose (D_e) Overdispersion (Ov), Dose Recovery (DRec), Overdisperion in dose recovery (Ov Drec). D_es marked with * mean that the Central Age Model was used. Rejected ages are in red *italics*.

Sample	D_r (mGy/a)	N	D_e (Gy)	Ov. (%)	D_{rec}	Ov. D_{rec} (%)	Age (a)	Environment
H1	0.62 ± 0.04	33	6.72 ± 1.93	56.6 ± 9.4	1.10 ± 0.05	8 ± 4	10,837 ± 3178	Lake
H2	0.83 ± 0.05	33	10.87 ± 0.79	60.1 ± 8.7	0.94 ± 0.03	3 ± 6	13,121 ± 1232	Lake
H3	0.74 ± 0.04	40	10.17 ± 1.94	63.1 ± 15.2	1.00 ± 0.04	8 ± 4	13,709 ± 2716	Lake
H4	0.99 ± 0.04	34	13.58 ± 0.89	76.0 ± 9.8	0.99 ± 0.04	10 ± 4	13,667 ± 1043	Lake
H5	1.23 ± 0.05	34	17.05 ± 1.21	68.6 ± 10.5	0.97 ± 0.06	18 ± 5	13,915 ± 1118	Lake
H6	1.49 ± 0.06	38	9.66 ± 0.48	65.9 ± 8.4	1.01 ± 0.03	4 ± 4	6489 ± 413	Lake
H7	1.12 ± 0.04	33	4.93 ± 0.48	58.5 ± 8.1	0.95 ± 0.08	19 ± 6	4418 ± 500	T7 Cunas
H8	0.89 ± 0.02	32	10.58 ± 1.28	53.2 ± 7.7	0.99 ± 0.03	7 ± 4	11,871 ± 1470	Lake
H9	0.90 ± 0.04	31	3.75 ± 0.87	83.3 ± 11.7	0.91 ± 0.05	14 ± 5	4153 ± 988	T7 Cunas
H10	1.17 ± 0.11	32	12.10 ± 0.79	55.3 ± 8.0	1.03 ± 0.07	19 ± 5	10,326 ± 1188	Lake
H11	1.10 ± 0.04	35	0.14 ± 0.05	83.2 ± 10.6	0.87 ± 0.04	13 ± 1	131 ± 46	T1B Cunas
H12	1.73 ± 0.08	38	3.88 ± 0.33*	48.0 ± 7.5	1.01 ± 0.03	5 ± 3	2245 ± 217	T6 Cunas
H13	1.56 ± 0.09	33	2.69 ± 0.39	69.8 ± 8.5	–	–	*1722 ± 268*	T2 Cunas
H15	1.06 ± 0.05	46	1.70 ± 0.45	32.9 ± 4.5	1.15 ± 0.06	10 ± 5	1604 ± 434	T4B Cunas
H16	0.69 ± 0.03	44	4.38 ± 0.31	42.7 ± 4.9	1.01 ± 0.01	24 ± 8	6326 ± 519	T7 Cunas?
H17	1.05 ± 0.04	14	51.37 ± 17.67	37.6 ± 9.5	–	–	*49,009 ± 16,966*	T5 Cunas
H19	1.73 ± 0.07	35	1.43 ± 0.10*	35.5 ± 5.7	0.97 ± 0.10	29 ± 8	824 ± 66	T3C Cunas
H20	1.82 ± 0.05	37	2.16 ± 0.14*	37.8 ± 5.1	1.13 ± 0.05	10 ± 4	1188 ± 86	T4A Cunas
H22	1.27 ± 0.06	46	12.81 ± 0.78	50.5 ± 5.9	–	–	*10,077 ± 803*	T7 Cunas
H23	1.40 ± 0.30	37	0.36 ± 0.09	68.7 ± 9.1	1.08 ± 0.04	9 ± 3	255 ± 87	T2 Cunas
M1	1.68 ± 0.05	31	4.30 ± 0.78	67.1 ± 9.2	1.00 ± 0.05	11 ± 5	2564 ± 469	T4 Mantaro
M2	2.45 ± 0.08	43	1.24 ± 0.16	91.1 ± 10.1	0.86 ± 0.07	13 ± 1	507 ± 67	T3 Mantaro

Table 6
Results of the radiocarbon dating of samples: isotope fractionation ($\delta^{13}C$), C:N ratio, percentage of modern carbon (pMC), uncalibrated and calibrated ages. "B·P" means years before the year 1950. Rejected ages are in red *italics*.

Sample	Lab code	$\delta^{13}C$ (‰)	C:N	14C Age (y BP)	Cal Age 2σ (BP)	Environment
H1	18OS/094	−26.25	1.83	10,220 ± 40	11,932 ± 165	Lake
H2	18OS/0807	−22.11	1.41	10,300 ± 40	12,113 ± 268	Lake
H5	18OS/0808	+1.56	0.92	10,320 ± 60	12,122 ± 283	Lake
H7	18OS/0947	+0.003	3.01	8870 ± 40	*9978 ± 196*	T7 Cunas
H9	18OS/0948	−2.43	2.86	2220 ± 30	*2238 ± 86*	T7 Cunas
H12	18OS/0949	−4.00	13.01	3220 ± 30	*3206 ± 129*	T6 Cunas
H13	18OS/0814	−19.16	10.96	3010 ± 30	*3464 ± 54*	T2 Cunas
H15	18OS/0950	−3.79	8.42	4990 ± 40	*5750 ± 140*	T4B Cunas

240-year cyclicity during the past millennia in which precipitation increased by at least 8% and which may be linked to changes in Atlantic sea surface temperatures (SST) controlling the intensity of the SASM (Baker et al., 2009). A 216-year, insolation-forced climate cyclicity was also identified in fluxes of clastic material in the Chochos Lagoon in north eastern Peru (Bush et al., 2005). Our OSL ages of the terrace sediments in the Cunas River show that terraces were formed approximately every 250 to 300 years from 2245 ± 217 years ago until 1188 ± 60 years ago (T6 to T3C) and approximately every 150 years after 824 ± 66 yrs. ago and until the present (Figs.7 and 9), thereby reinforcing the idea that cyclic changes in the SASM were controlling the deposition of the fluvial sediments.

6.2. Factors controlling fluvial incision

Whilst the cyclicity in SASM may explain the variations in river discharge and the deposition of fluvial sediments in the Mantaro and Cunas valleys, it cannot account for the observed incision in both valleys. It has been shown that base-level lowering is a prerequisite for terrace formation (Blum and Törnqvist, 2000; Bridgland and Westaway, 2008b; Viveen et al., 2013a). Sea-level changes as a driving factor can be discarded as the Mantaro watershed drains to the Atlantic Ocean, which is situated too far away to be of any significant influence, and sea-level has not changed significantly during the Holocene. Draining of the sediment-filled lake that occupied the Mantaro valley may have been a cause for incision, as base-level suddenly dropped and both rivers had to adapt to a new base-level. Similar situations have been described for the mayor river systems in Spain (Antón et al., 2012). Base-level changes may also be controlled by tectonic uplift (Bridgland and Westaway, 2008b; Viveen et al., 2013b; Viveen et al., 2014b). The Huancayo basin is tectonically active and short-lived compressive events occur. This is corroborated by the registration of small seismic events in the instrumental record (Tavera, 2017). However, these short-lived events cause brittle deformation of the sediments and cannot be responsible for long-term uplift of the area. A second line of evidence for long-term uplift stems from the asymmetrically developed terraces and the presence of the folds on the western basin margin (Figs. 2 and 4), as well as overthursting of the basin border by Mesozoic rocks (Wise, 2007). Ongoing folding may cause regional-scale uplift and preservation of fluvial terraces (Bridgland and Westaway, 2008b). However, numerical modelling experiments have shown that terrace threads tend to diverge where folding is most intense (Geach et al., 2015). Our reconstruction of terrace threads in the Cunas valley shows that the terraces trend parallel to one another without diverging towards the western basin border, where folding is most intense (Fig. 10). We also observed that, in the vicinity of the folds close to the border, the Mantaro terraces are only locally deformed. The fold mapped in the Mantaro T5 terrace was not investigated in the field by us, but we suggest that the fold is most likely an inherited feature connected to the older rocks underlying the lacustrine sediments. We deem it highly unlikely that a 50 m-high fold has formed in a terrace surface of Holocene age. The fold is also cut by the T4 Mantaro terrace, suggesting it formed much earlier. Incision rates are often used as a proxy for tectonic uplift (Bridgland and Westaway, 2008b). In the Cunas valley, 34 m of incision occurred over the past 4418 ± 500 years, averaging 7.7 mm yr^{-1} thereby assuming that incision has kept pace with uplift. For comparison, the southern Peruvian coast, where active underthursting of the Nazca Ridge takes place, the average middle–late Pleistocene uplift rate is 0.4 to 0.9 mm yr^{-1} (Saillard et al., 2011). Similarly, in the Moquegua valley of southern Peru (18° S), only three terrace levels have formed since 2178 years ago, with the oldest terrace seven metres above the floodplain (Magilligan et al., 2008). The Moquegua area is characterised by one of the highest uplift rates of the Peruvian Andes (Noury et al., 2016), yet it has hardly affected the vertical position of the fluvial terraces. We cannot think of any geodynamic reason why the uplift in the Huancayo basin should be an order of magnitude higher when compared to other, tectonically highly active regions in Peru. For those reasons we discard folding and tectonic uplift in general as a primary mechanism for inducing relative base-level fall, although it may be a secondary contributing factor. Another reason for base-level lowering could be the change from endorheic to exoreic conditions of the Huancayo basin over longer timescales as postulated by Wise (2007) and Wise and Noble (2008). The Mantaro and Cunas River terraces that were formed between 4418 ± 500 yrs. ago and the present have a similar number of fluvial terraces and are located at similar heights above their respective floodplains (Fig. 10). The terrace threads of the Cunas River have also a more-or-less equal vertical spacing of approximately five metres between them and they trend parallel to one another. The Cunas River (Fig. 10), as well as the Mantaro River (Wise and Noble, 2008), also have straight channel shapes. All this suggests that both rivers are actively grading towards a shared base-level that is situated outside of the Huancayo basin, e.g. the Amazon catchment. This is also corroborated by the constant accumulative incision rates of 6 mm yr^{-1} after 2245 ± 217 years ago (Fig. 15) showing little to no variation, thereby fostering the idea of a regional instead of local (e.g. tectonic) control. These very high incision rates suggest that the Huancayo basin may not have become an externally-drained basin during the lower Pleistocene as was suggested by Wise (2007) on the basis of very limited dating evidence. By now the basin should have graded towards its new base-level. The Mantaro T5 terrace surface is also much younger (4418 ± 500 years) instead of being from the second (e.g. Saalien) glaciation (Mégard, 1968). We therefore suggest that the basin is much younger, for instance middle to late Pleistocene in age. In summary, we propose that incision is primarily related to a short-term (Holocene) adjustment to a new base-level as well as a long-term adjustment (Pleistocene) induced by changes from endorheic to exoreic conditions. Deposition on the other hand, seems to have been controlled by centennial-scale fluctuations in the SASM.

6.3. A synchronous response of Peruvian Andean rivers to centennial variations in SASM

The little published information available suggests similar climatic

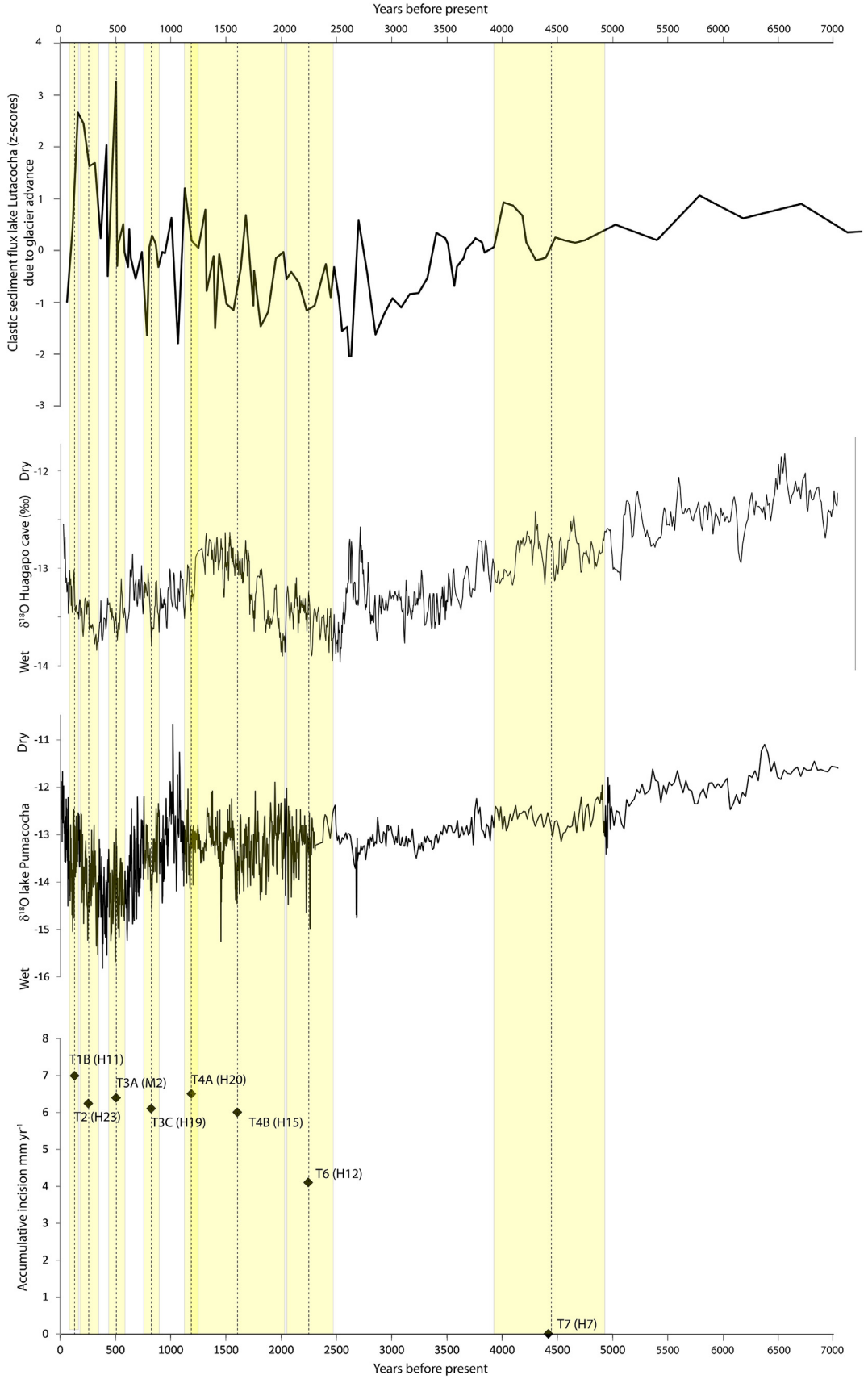

(caption on next page)

Fig. 15. Paleoclimatological reconstructions of the central Peruvian Andes. All records are located approximately 50 to 100 km northwest of the Huancayo basin. The records include z-scores of clastic sediment fluxes due to glacier advances in Lutacocha proglacial lake (Stansell et al., 2013); $\delta^{18}O$ isotopic values of a speleothem record of Huapago cave as a proxy for precipitation (Kanner et al., 2013); and $\delta^{18}O$ isotopic values of Pumacocha lake sediments as a proxy for precipitation (Bird et al., 2011). Cunas and Mantaro River OSL ages in combination with the accumulative incision up to the moment of terrace formation in lower section. Dotted lines indicate age of Cunas and Mantaro terraces and yellow fields the error of the age estimates. Note excellent correspondance between terrace ages, wet periods and moments of glacier retreat. (For interpretation of the references to colour in this figure legend, the reader is referred to the web version of this article.)

Table 7
Comparison of flood event ages of different river systems in the Peruvian Andes. Ages from Wells (1990), Keefer et al. (2003) and Magilligan et al. (2008) are given in years before present, where the present is set at the year 2018. This makes it possible to compare the radiocarbon ages of these authors directly with our OSL ages. Note good correspondence between the different flood events dated.

Wells (1990)		Keefer et al. (2003)		Magilligan et al. (2008)		This paper	
Age	Site	Age interval	Site	Age	Site	Age	Terrace
n.a.	n.a.	4215–3115	Yara	4240 ± 150	Yaral	4418 ± 500	T7
3288 ± 130	Casma River	4215–3115	Yara	3250 ± 70	Alluvial fan	n.a.	n.a.
2018 ± 130	Casma River	n.a.	n.a.	2178 ± 40	Conde high terrace	2245 ± 217	T6
n.a.	n.a.	n.a.	n.a.	1868 ± 40	Conde high terrace	T5?	T5?
n.a.	n.a.	n.a.	n.a.	n.a.	n.a.	1604 ± 434	T4B
n.a.	n.a.	n.a.	n.a.	1328 ± 40	Conde high terrace	n.a.	n.a.
n.a.	n.a.	n.a.	n.a.	1118 ± 70	Conde high terrace	1188 ± 60	T4A
n.a.	n.a.	n.a.	n.a.	788 ± 50	Conde middle terrace	824 ± 66	T3C
688 ± 60	Casma River	718–618	Miraflores	728 ± 50	Conde middle terrace	T3B?	T3B?
564 ± 20	Casma River	n.a.	n.a.	608 ± 40	Conde high terrace	507 ± 67	T3 Mantaro?
480 ± 69	Medio Mundo	410–411	Chuza	418 ± ?	Conde low terrace	n.a.	n.a
282 ± 71	Casma River	n.a.	n.a.	208 ± 140	Los Espejos gravels	255 ± 87	T2
150 ± 53	Casma River	n.a.	n.a.	208 ± 140	Los Espejos gravels	131 ± 46	T1B
88 ± 50	Casma River	n.a.	n.a.	n.a.	n.a.	T1A?	T1A?

mechanisms for terrace formation elsewhere in the Peruvian Andes during the late Holocene. In the Llave River valley on the Altiplano, five fluvial terraces were formed. The three oldest were formed before 8300 years BP and the two youngest between 4000 and 2500 and 2000–1600 years BP (Rigsby et al., 2003). Formation of the youngest terraces corresponds to rising lake levels on the Altiplano, suggesting an increasingly more humid climate (Rigsby et al., 2003). It is striking that the two youngest terraces were formed at the two key times recorded in the Cunas-Mantaro valley: the moment of renewed valley formation dated at 4418 ± 500 years ago and the moment of accelerated incision and terrace formation dated at 2245 ± 217 years ago. Similarly, in the Ilo valley (18° S latitude), bordering Chile, three debris-flow deposits were dated at the same time as terrace formation in the Cunas valley (Keefer et al., 2003; Table 7). Strong parallels also exist between our study area and the Moquegua River valley (18° S latitude; Table 7). Here, a detailed record of stacked fluvial flood deposits exists that is incorporated in three terrace levels and that was linked to periods of ENSO-controlled increased precipitation (Magilligan et al., 2008). At Yaral, in an archaeological complex on top of a gravelly fluvial terrace, a major flood was registered between 4390 and 4090 years ago after an absence of floods during the early–middle Holocene. The next event, which was not recognised in our record, was the deposition of an alluvial fan at 3250 ± 70 years ago. The most complete record for flood events exists in the Conde High terrace complex. Here, the onset of the most important phase of flood events started at 2178 ± 40 years ago, which agrees very well with the initiation of the terrace sequence in the Cunas River valley at 2245 ± 217 years ago, and which lasted until 418 years ago (Table 7). A total of 13 events were recognised since 2178 ± 40 years ago, with an increase in flood frequency towards the present: one flood per 270 years from 1868 to 1328 years ago and one flood per 120 years between 1328 and 608 yrs. ago. The overall average is of one flood per 170 years over the past 2178 yrs. (Magilligan et al., 2008). Not only is the frequency of flooding very similar to that in the Cunas and Mantaro valleys, but also the timing of sedimentation is very similar (Table 7), showing the regional importance of variations in precipitation on fluvial sedimentation. Similarly, a history of precipitation-induced flooding for the Casma region (central Peruvian coast at 10° S) shows that the two major floods occurred at approximately 3200 years ago and 2018 ± 130 years ago (Wells, 1990; Table 7). After that the frequency of flooding increased drastically with a frequency of 125 years per event between 693 years ago and 140 years ago, just like in our study area (Wells, 1990). Both Wells (1990) and Magilligan et al. (2008) attribute the late Holocene variations in precipitation to ENSO events. But Baker and Fritz (2015) point out that, while ENSO is the most important mechanism for interannual variations in air temperature and for some regions partly explains the fluctuations in precipitation patterns, there is no significant statistic correlation with precipitation and flood events during the SASM period in the instrumental record. A statistical analysis of the correlation between ENSO and rainfall in the Mantaro basin, on the basis of precipitation data from 1970 to 2004, also shows a very weak negative correlation of −0.34, indicating that ENSO does not control precipitation in our study area (Silva et al., 2008). Over timescales spanning centuries to millennia, there is disagreement between the onset, duration and intensity of ENSO in the different paleoclimatic archives (Vuille et al., 2012; Baker and Fritz, 2015). Instead, centennial-to millennial-scale oscillations in the SASM have been primarily linked to changes in the position of the ITCZ in which a southward shift in the ITCZ led to increased precipitation over South America and a northward shift to a decrease in precipitation (Bird et al., 2011b; Vuille et al., 2012; Kanner et al., 2013; Stansell et al., 2013). The position of the ITCZ in turn is thought to be controlled by changes in North Atlantic SST (Vuille et al., 2012; Apaéstegui et al., 2014; Baker and Fritz, 2015; Bustamante et al., 2016). A warming of North Atlantic SST results in a smaller temperature gradient between ocean and atmosphere, thereby weakening the Hadley cell of the northern hemisphere and causing a northward displacement of the ITCZ; a decrease in SST results in a strengthened Hadley cell and a southward shift of the ITCZ (Baker et al., 2001a; Wu et al., 2019). A statistically significant correlation was also found between rainfall in the Mantaro basin and the Tropical Atlantic SST for the past decades (IGP, 2005; Silva et al., 2008). The similarities between our fluvial record and those of Wells (1990), Keefer et al. (2003) and Magilligan et al. (2008) therefore suggest that it is not ENSO that is responsible for the observed centennial-scale pattern in deposition of fluvial sediments, but rather oscillations in the SASM, modulated by a southward shift of the ITCZ, which in turn is linked to changes in North

Atlantic SST. In conclusion, the few little data available suggest that, during the Holocene, fluvial systems in various parts of the Peruvian Andes have responded synchronously to centennial-scale changes in SASM intensity and frequency.

7. Conclusions

Sedimentological and stratigraphical evidence, in combination with geomorphological mapping and radiometric dating, shows that in the Mantaro valley an ephemeral lake was present from at least 12,000 years ago until shortly before 4418 ± 500 years ago. Draining of the lake resulted in opening up of the contemporary Mantaro and Cunas River valleys. The timing of valley opening coincided with a retreat of glaciers in the central Peruvian Andes and with the onset of a higher frequency of SASM events when compared to the middle Holocene. The timing of SASM events characterised by increased precipitation coincides with the deposition of fluvial sediments. The majority of fluvial terraces were formed between 2245 ± 217 years ago and the present, coinciding with the period of highest frequency of SASM events since the beginning of the Holocene. The deposits were subsequently incised by the rivers under a regime of continuous adjustment to a new base-level. Base-level fall occurred due to changes from endorheic to exoreic conditions at at least two different times in the Pleistocene and late Holocene. A comparison with fluvial data from other rivers in the Peruvian Andes shows strong similarities in the frequency and timing of flooding and deposition. The centennial-scale cyclicity of flooding and deposition shows that changes in ENSO activity are not responsible, but instead the driver was changes in SASM intensity controlled by displacements of the ITCZ.

Acknowledgements

This paper benefitted from funding from the Dirección de Gestión de la Investigación de la Pontificia Universidad Católica del Perú (PUCP): Proyecto Especial 399. It also benefitted from funding from the University of A Coruña which permitted Willem Viveen to visit the University of A Coruña. Finally, a grant from the Dirección Académica de Relaciones Institucionales of the PUCP permitted Jorge Sanjurjo Sanchez to spend time at the PUCP and to work on this paper. Guest editor David Bridgland and two anonymous reviewers are kindly acknowledged for helpful comments that improved the manuscript.

References

Abbühl, L.M., Norton, K.P., Schlunegger, F., Kracht, O., Aldahan, A., Possnert, G., 2010. El Niño forcing on 10Be-based surface denudation rates in the northwestern Peruvian Andes? Geomorphology 123, 257–268.

Accoe, F., Boeckx, P., Van Cleemput, O., Hofman, G., Hui, X., Bin, H., Guanxiong, C., 2002. Characterizatioon of soil organic matter fractions from grassland and cultivated soils via C content and $\delta^{13}C$ signature. Rapid Commun. Mass Spectrom. 16, 2157–2164.

Antón, L., Rodés, A., De Vicente, G., Pallàs, R., Garcia-Castellanos, D., Stuart, F.M., Braucher, R., Bourlès, D., 2012. Quantification of fluvial incision in the Duero Basin (NW Iberia) from longitudinal profile analysis and terrestrial cosmogenic nuclide concentrations. Geomorphology 165-166, 50–61.

Apaéstegui, J., Cruz, F.W., Sifeddine, A., Vuille, M., Espinoza, J.C., Guyot, J.L., Khodri, M., Strikis, N., Santos, R.V., Cheng, H., Edwards, L., Carvalho, E., Santini, W., 2014. Hydroclimate variability of the northwestern Amazon Basin near the Andean foothills of Peru related to the South American monsoon system during the last 1600 years. Clim. Past 10, 1967–1981.

Baker, P.A., Fritz, S.C., 2015. Nature and causes of Quaternary climate variation of tropical South America. Quat. Sci. Rev. 124, 31–47.

Baker, P.A., Rigsby, C.A., Seltzer, G.O., Fritz, S.C., Lowenstein, T.K., Bacher, N.P., Veliz, C., 2001a. Tropical climate changes at millennial and orbital timescales in the Bolivian Altiplano. Nature 409, 698–701.

Baker, P.A., Seltzer, G.O., Fritz, S.C., Dunbar, R.B., Grove, M.J., Tapia, P.M., Cross, S.L., Rowe, H.D., Broda, J.P., 2001b. The history of South American tropical precipitation for the past 25,000 years. Science 291, 640–643.

Baker, P.A., Fritz, S.C., Burns, S.J., Ekdahl, E., Rigsby, C.A., 2009. The nature and origin of decadal to millennial scale climate variability in the southern tropics of South America. In: Vimeux, F., Sylvestre, F., Khodri, M. (Eds.), Past Climate Variability from the Last Glacial Maximum to the Holocene in South America and Surrounding Regions. Springer, NY, pp. 301–322.

Ballarini, M., Wallinga, J., Murray, A.S., van Heteren, S., Oost, A.P., Bos, A.J.J., van Eijk, C.W.E., 2003. Optical dating of young coastal dunes on a decadal time scale. Quat. Sci. Rev. 22, 1011–1017.

Bekaddour, T., Schlunegger, F., Vogel, H., Delunel, R., Norton, K.P., Akcar, N., Kubik, P., 2014. Paleo erosion rates and climate shifts recorded by Quaternary cut-and-fill sequences in the Pisco valley, Central Peru. Earth Planet. Sci. Lett. 390, 103–115.

Bird, B.W., Abbott, M.B., Rodbell, D.T., Vuille, M., 2011. Holocene tropical South American hydroclimate revealed from a decadally resolved lake sediment $\delta^{18}O$ record. Earth Planet. Sci. Lett. 310, 192–202.

Blanc, J.L., 1984. Néotectonique et Sismotectonique des Andes du Perou central dans la région de Huancayo. These Docteur 3éme Cycle, Université de Paris-Sud. Centre d'Orsay 161, 10.

Blum, M.D., Törnqvist, T.E., 2000. Fluvial response to climate and sea-level change: a review and look forward. Sedimentology 47 (Suppl. 1), 2–48.

Brennan, B.J., 2003. Beta doses to spherical granis. Radiat. Meas. 3, 299–303.

Bridgland, D., Westaway, R., 2008a. Climatically controlled river terrace staircases: a worldwide Quaternary phenomenon. Geomorphology 98, 285–315.

Bridgland, D.R., Westaway, R., 2008b. Preservation patterns of late Cenozoic fluvial deposits and their implications: results from IGCP 449. Quat. Int. 189, 5–38.

Bronk Ramsey, C., Lee, S., 2013. Recent and planned developments of the program OxCal. Radiocarbon 55 (2–3), 720–730.

Bush, M.B., Hansen, B.C.S., Rodbell, D.T., Seltzer, G.O., Young, K.R., León, B., Abbott, M.B., Silman, M.R., Gosling, W.D., 2005. A 17,000-year history of Andean climate and vegetation change from Laguna de Chochos, Peru. J. Quat. Sci. 20, 703–714.

Bustamante, M.G., Cruz, F.W., Siffedine, A., Cheng, H., Apaéstegui, J., Vuille, M., Strikis, N., Moquet, J.S., Novello, V.F., Guyot, J., Edwards, L., 2016. Holocene changes in monsoon precipitation in the Andes of NE Peru based on δ18O speleothem records. Quat. Sci. Rev. https://doi.org/10.1016/j.quascirev.2016.05.023.

Chiang, J.C.H., Bitz, C.M., 2005. Influence of high latitude ice cover on the marine Intertropical Convergence Zone. Clim. Dyn. 25, 477–496.

Deines, P., 1980. The isotopic composition of reduced organic carbon. In: Fritz, P., Fontes, J.C. (Eds.), Handbook of Environmental Isotope Geochemistry. vol. 1. Elsevier, Amsterdam, pp. 329–406 The terrestrial environment.

Dorbath, C., Dorbath, L., Cisternas, A., Deverchère, J., Sebrier, M., 1990. Seismicity of the Huancayo Basin (Central Peru) and the Huaytapallana fault. J. S. Am. Earth Sci. 3 (1), 21–29.

Ferro-Vázquez, C., Kaal, J., Santos Arévalo, F.J., Criado Boado, F., 2018. Molecular fingerprinting of 14C dated soil organic matter fractions from archaeological settings in NW Spain. Radiocarbon 2018https://doi.org/10.1017/RDC.2018.62. online.

Galbraith, R.F., Roberts, R.G., Laslett, G.M., Yoshida, H.Y., Olley, H., 1999. Optical Dating of Single and Multiple Grains of Quartz from Jinmium Rock Sherlter, Northern Australia: Part 1, Archaeometry. vol. 41. pp. 339–364.

Garreaud, R., Vuille, M., Clement, A., 2003. The climate of the Altiplano: observed current conditions and mechanisms of past changes. Palaeogeogr. Palaeoclimatol. Palaeoecol. 194, 5–22.

Garreaud, R.D., Vuille, M., Compagnucci, R., Marengo, J.A., 2009. Present-day south American climate. Palaeogeogr. Palaeoclimatol. Palaeoecol. 281, 180–195.

Gayo, E.M., Latorre, C., Santoro, C.M., Maldonado, A., De Pol-Holz, R., 2012. Hydroclimate variability in the low-elevation Atacama Desert over the last 2500 yr. Clim. Past 8, 287–306.

Geach, M., Viveen, W., Mather, A.E., Stokes, M., Telfer, M.W., Fletcher, W., 2015. An integrated field and modelling study of controls on late Quaternary fluvial landscape development (Tabernas, SE Spain). Earth Surf. Process. Landf. 40, 1907–1926.

Guerin, G., Mercier, N., Adamiec, G., 2011. Dose-rate conversión factors: update. Ancient TL 29, 5–8.

Harrison, J.V., 1943. Geología de los Andes centrales en parte del departamento de Junín, Perú. Boletín Sociedad Geológica del Perú 16, 1–52.

Howard, A.J., Gearey, B.R., Hill, T., Fletcher, W., Marshall, P., 2009. Fluvial sediments, correlations and palaeoenvironmental reconstruction: the development of robust radiocarbon chronologies. J. Archaeol. Sci. 36, 2680–2688.

Hurrell, J.W., van Loon, H., 1997. Decadal variations in climate associated with the North Atlantic Oscillation. Clim. Chang. 36, 301–326.

IGP, 2005. Vulnerabilidad y adaptación al cambio climático en la cuenca del río Mantaro. Fondo Editorial CONAM, Lima, Peru.

Kanner, L.C., Burns, S.J., Cheng, H., Edwards, R.L., Vuille, M., 2013. High-resolution variability of the south American summer monsoon over the last seven millennia: insights from a speleothem record from the central Peruvian Andes. Quat. Sci. Rev. 75, 1–10.

Keefer, D.K., Moseley, M.E., de France, S.D., 2003. A 38 000-year record of £oods and debris flows in the Ilo region of southern Peru and its relation to El Niño events and great earthquakes 2003. Palaeogeogr. Palaeoclimatol. Palaeoecol. 194, 41–77.

Litty, C., Lanari, P., Burn, M., Schlunegger, F., 2017a. Climate-controlled shifts in sediment provenance inferred from detrital zircon ages, western Peruvian Andes. Geology 45 (1), 59–62.

Litty, C., Schlunegger, F., Viveen, W., 2017b. Possible threshold controls on sediment grain properties of Peruvian coastal river basins. Earth Surf. Dyn. 5, 571–583.

Litty, C., Schlunegger, F., Akcar, N., Delunel, R., Christl, M., Vockenhuber, C., 2018. Chronology of alluvial terrace sediment accumulation and incision in the Pativilca valley, western Peruvian Andes. Geomorphology 315, 45–56.

Madsen, A.T., Murray, A.S., 2009. Optically stimulated luminescence dating of young sediments: a review. Geomorphology 109 (1–2), 3–16.

Magilligan, F.J., Goldstein, P.S., Fisher, G.B., Bostick, B.C., Manners, R.B., 2008. Late Quaternary hydroclimatology of a hyper-arid Andean watershed: climate change, floods, and hydrologic responses to the El Niño-Southern oscillation in the Atacama Desert. Geomorphology 101, 14–32.

Marocco, R., Lavenu, A., Baudino, R., 1995. Intermontane late Paleogene –Neogene basins of the Andes of Ecuador and Peru: sedimentologic and tectonic characteristics. In: Tankard, A.J., Suarez, S.R., Welsink, H.J. (Eds.), Petroleum basins of South America. American Association of Petroleum Geologists Memoir. 62. pp. 597–613.
Mayya, Y.S., Morthekai, P., Murari, M.K., Singhvi, A.K., 2006. Towards quantifying beta microdosimetric effects in single-grain quartz dose distribution. Radiat. Meas. 41, 1032–1039.
Mégard, F., 1968. Geología del cuadrángulo de Huancayo. Bol. Del Servicio de Geológía y Minería 18. Lima. Peru 18, 1–123.
Meyers, P.A., 1994. Preservation of elemental and isotopic source identification of sedimentary organic matter. Chem. Geol. 114, 289–302.
Miall, A.D., 1996. The Geology of Fluvial Deposits: Sedimentary Facies, Basin Analysis and Petroleum Geology. Springer, New York, pp. 598.
Ministerio de Agricultura, ANA, 2010. Administración Local de Agua Mantaro. Evaluación de recursos hídricos superficiales en la cuenca del río Mantaro, Lima, Peru, pp. 137.
Ministerio de Agricultura and ANA, 2013. Atlas de Recursos Hídricos Del Perú. AAA Mantaro, Lima, Peru, pp. 237–260.
Murray, A.S., Wintle, A.G., 2000. Luminescence dating of quartz using an improved single-aliquot regenerative-dose protocol. Radiat. Meas. 32, 57–73.
Murray, A.S., Wintle, A.G., 2003. The single aliquot regenerative dose protocol: potential for improvements in reliability. Radiat. Meas. 37, 377–381.
Nanson, G.C., Croke, J.C., 1992. A genetic classification of floodplains. Geomorphology 4, 459–486.
Nichols, G., 2009. Sedimentology and Stratigraphy, 2nd ed. Wiley-Blackwell, Oxford, pp. 419.
Nobre, P., Shukla, J., 1996. Variations of sea surface temperature, wind stress, and rainfall over the tropical Atlantic and South America. J. Clim. 9, 2464–2479.
Noury, M., Bernet, M., Schildgen, T.F., Simon-Labric, T., Philippon, M., Sempere, T., 2016. Crustal-scale block tilting during Andean trench-parallel extension: structural and geo-thermochronological insights. Tectonics 35. https://doi.org/10.1002/2016TC004231.
Paredes, J., 1970. Geología Del Cuadrángulo de Jauja, hoja 24-m. Boletin 48. Instituto Geológico Minero Metalúrgico, Lima, Peru, pp. 113.
Prescott, J.R., Hutton, J.T., 1994. Cosmic ray contributions to dose rates for luminescence and ESR dating: large depths and long term variations. Radiat. Meas. 23, 497–500.
Reimer, P.J., Bard, E., Bayliss, A., Beck, J.W., Blackwell, P.G., Bronk Ramsey, C., Grootes, P.M., Guilderson, T.P., Haflidason, H., Hajdas, I., Hattž, C., Heaton, T.J., Hoffmann, D.L., Hogg, A.G., Hughen, K.A., Kaiser, K.F., Kromer, B., Manning, S.W., Niu, M., Reimer, R.W., Richards, D.A., Scott, E.M., Southon, J.R., Staff, R.A., Turney, C.S.M., Van Der Plicht, J., 2013. IntCal13 and marine13 radiocarbon age calibration curves 0-50,000 years cal BP. Radiocarbon 55, 1869–1887.
Rein, B., Luckage, A., Sirocko, F., 2004. A major Holocene ENSO anomaly during the medieval period. Geophys. Res. Lett. 31, L17211.
Rein, B., Luckage, A., Reinhardt, L., Sirocko, F., Wolf, A., Dullo, W.C., 2005. El Niño variability off Peru during the last 20,000 years. Palaeoceanography 20 (2004) (PA001099).
Rigsby, C.A., Baker, P.A., Aldenderfer, M.S., 2003. Fluvial history of the Rio Ilave valley, Peru, and its relationship to climate and human history. Palaeogeogr, Palaeoclimatol, Paleoecol. 3061, 1–21.
Saillard, M., Hall, S.R., Audin, L., Farber, D.L., Regard, V., Hérail, G., 2011. Andean Coastal Uplift and Active Tectonics in Southern Peru: 10Be Surface Exposure Dating of Differentially Uplifted Marine Terrace Sequences (San Juan de Marcona, ~15.4°S).
Sandweiss, D.H., Shady Solis, R., Moseley, M.E., Keefer, D.K., Ortloff, C.R., 2009. Environmental change and economic development in coastal Peru between 5,800 and 3,600 years ago. PNAS. https://doi.org/10.1073/pnas.0812645106.
Schittek, K., Forbriger, M., Mächtle, B., Schäbitz, F., Wennrich, V., Reindel, M., Eitel, B., 2015. Holocene environmental changes in the highlands of the southern Peruvian Andes (14° S) and their impact on pre-Columbian cultures. Clim. Past 11, 27–44.
Seager, R., Kushnir, Y., Visbeck, M., et al., 2000. Causes of Atlantic Ocean climate variability between 1958 and 1998. J. Clim. 13, 2845–2862.
Seltzer, G.O., Hastorf, C.A., 1990. Climatic change and its effect on prehispanic agriculture in the central Peruvian Andes. J. Field Archaeol. 17 (4), 397–414.
Seltzer, G., Rodbell, D., Burns, S., 2000. Isotopic evidence for late Quaternary climate change in tropical South America. Geology 28 (1), 35–38.
Silva, Y., Takahasi, K., Chávez, R., 2008. Dry and wet rainy seasons in the Mantaro river basin (Central Peruvian Andes). Adv. Geosci. 14, 261–264.
Stansell, N.D., Rodbell, D.T., Abbott, M.B., Mark, B.G., 2013. Proglacial lake sediment records of Holocene climate change in the western Cordillera of Peru. Quat. Sci. Rev. 70, 1–14.
Steffen, D., Schlunegger, F., Preusser, F., 2009. Drainage basin response to climate change in the Pisco valley, Peru. Geology 37 (6), 491–494.
Steffen, D., Schlunegger, F., Preusser, F., 2010. Late Pleistocene fans and terraces in the Majes valley, southern Peru, and their relation to climatic variations. Int. J. Earth Sci. (Geol Rundsch) 99, 1975–1989.
Tavera, H., 2017. Mapa sísmico del Perú. Periodo. Ministerio del Ambiente y Instituto Geofísico del Perú, Lima, Perú, pp. 1960–2016.
Vandenberghe, J., Bridgland, D., Wang, X., 2018. Specific exogenetic (external) and endogenetic (internal) effects on fluvial system evolution. Quaternary 1, 27. https://doi.org/10.3390/quat1030027.
Veldkamp, A., Baartman, J., Coulthard, T., Maddy, D., Schoorl, J., Storms, J., Temme, A., van Balen, R., van de Wiel, M., van Gorp, W., Viveen, W., Westaway, R., Whittaker, A., 2017. Two decades of numerical modelling to understand long term fluvial archives: advances and future perspectives. Quat. Sci. Rev. 166, 177–187.
Viveen, W., Schlunegger, F., 2018. Prolonged extension and subsidence of the Peruvian forearc during the Cenozoic. Tectonophysics 730, 48–62.
Viveen, W., Schoorl, J.M., Veldkamp, A., van Balen, R.T., Desprat, S., Vidal-Romani, J.R., 2013a. Reconstructing the interacting effects of base level, climate, and tectonic uplift in the lower Miño terrace record: a gradient modelling evaluation. Geomorphology 186, 96–118.
Viveen, W., Schoorl, J.M., Veldkamp, A., van Balen, R.T., Vidal-Romani, J.R., 2013b. Fluvial terraces of the NW Iberian lower Miño River. J. Maps 9 (4), 513–522.
Viveen, W., Sanjurjo-Sánchez, J., Goy-Diz, A., Veldkamp, A., Schoorl, J.M., 2014a. Paleofloods and ancient fishing weirs in NW Iberian rivers. Quat. Res. 82, 56–65.
Viveen, W., Schoorl, J.M., Veldkamp, A., van Balen, R.T., 2014b. Modelling the impact of regional uplift and local tectonics on fluvial terrace preservation. Geomorphology 210, 119–135.
Vuille, M., Burns, S.J., Taylor, B.E., Cruz, F.W., Bird, B.W., Abbott, M.B., Kanner, L.C., Cheng, H., Novello, V.F., 2012. A review of the south American monsoon history as recorded in stable isotopic proxies over the past two millennia. Clim. Past 8, 1309–1321.
Wang, Y., Hutington, T.G., Osher, L.J., Wassenaar, L.I., Trumbore, S.E., Amudson, R.G., Harden, J.H., McKnight, D.M., Schiff, S.L., Aiken, G.R., Lyons, W.B., Aravena, R.O., Baron, J.S., 1998. Carbon cycling in terrestrial environments. In: Kendall, C., McDonnell, J.J. (Eds.), Isotope Tracers in Catchment Hydrology. Elsevier, Amsterdam, pp. 577–610.
Wells, L.E., 1990. Holocene history of the El Ninño phenomenon as recorded in flood sediments of northern coastal Peru. Geology 18, 1134–1137.
Wise, J.M., 2007. Tectono-stratigraphic history of the Huancayo intermontane basin, Central Peru. Bol. Soc. Geol. Perú 102, 63–78.
Wise, J.M., Noble, D.C., 2008. Late Pliocene inception of external drainage and erosion of intermontane basins in the highlands of central Perú. Rev. Soc. Geol. Esp. 21 (1–2), 73–91.
Wu, C.-R., Lin, Y.-F., Qiu, B., 2019. Impact of the Atlantic multidecadal oscillation on the Pacific north equatorial current bifurcation. Nat. Sci. Rep. 9, 2162. https://doi.org/10.1038/s41598-019-38479-w.